



저작자표시-비영리-변경금지 2.0 대한민국

이용자는 아래의 조건을 따르는 경우에 한하여 자유롭게

- 이 저작물을 복제, 배포, 전송, 전시, 공연 및 방송할 수 있습니다.

다음과 같은 조건을 따라야 합니다:



저작자표시. 귀하는 원저작자를 표시하여야 합니다.



비영리. 귀하는 이 저작물을 영리 목적으로 이용할 수 없습니다.



변경금지. 귀하는 이 저작물을 개작, 변형 또는 가공할 수 없습니다.

- 귀하는, 이 저작물의 재이용이나 배포의 경우, 이 저작물에 적용된 이용허락조건을 명확하게 나타내어야 합니다.
- 저작권자로부터 별도의 허가를 받으면 이러한 조건들은 적용되지 않습니다.

저작권법에 따른 이용자의 권리는 위의 내용에 의하여 영향을 받지 않습니다.

이것은 [이용허락규약\(Legal Code\)](#)을 이해하기 쉽게 요약한 것입니다.

[Disclaimer](#)

Doctoral Thesis

Mechanisms for the Decadal Change of
the MJO Teleconnection over the Northern
Hemisphere in Boreal Winter

Hyerim Kim

Department of Urban and Environmental Engineering
(Environmental Science and Engineering)

Graduate School of UNIST

2020

Mechanisms for the Decadal Change of
the MJO Teleconnection over the Northern
Hemisphere in Boreal Winter

Hyerim Kim

Department of Urban and Environmental Engineering
(Environmental Science and Engineering)

Graduate School of UNIST

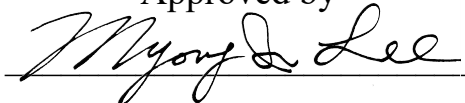
Mechanisms for the Decadal Change of
the MJO Teleconnection over the Northern
Hemisphere in Boreal Winter

A thesis/dissertation
submitted to the Graduate School of UNIST
in partial fulfillment of the
requirements for the degree of
Doctor of Philosophy

Hyerim Kim

December 17, 2019

Approved by



Advisor

Myong-In Lee

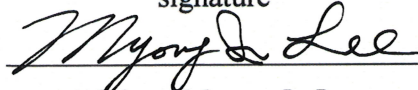
Mechanisms for the Decadal Change of
the MJO Teleconnection over the Northern
Hemisphere in Boreal Winter

Hyerim Kim

This certifies that the thesis/dissertation of Hyerim Kim is approved.

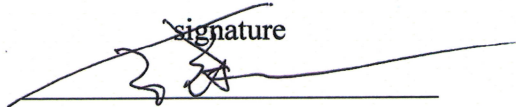
12.17.2019

signature



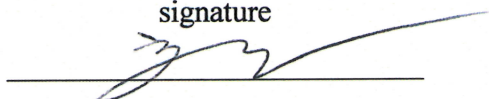
Advisor: Myong-In Lee

signature




Thesis Committee Member: ChangKeun Song

signature



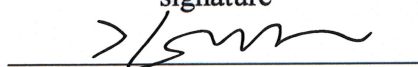
Thesis Committee Member: Dong-Hyun Cha

signature



Thesis Committee Member: Seokwoo Son

signature



Thesis Committee Member: Daehyun Kim

Abstract

This thesis suggests dynamical mechanisms for the decadal change of the MJO teleconnection pattern over the Northern Hemisphere during boreal winter by investigating the influence of the decadal change of background states in the mid-latitude and tropical forcing on MJO teleconnection pattern and interpreting this relationship.

Thus, it is important to understand how these changes influence on MJO teleconnection pattern to represent the MJO teleconnection pattern caused by changes of background states and MJO activities over the tropics. In boreal winter, OLR variance with intraseasonal variability variance is strengthened over the Maritime Continent and weakened over the southern Indian Ocean and the western Pacific. This is consistent with the results of the MJO amplitude at each MJO phase based on OMI. These changes of MJO activity are associated with the La Nina-like change of background states in tropics. There is wet and warm anomaly over the Maritime Continent and the western Pacific, and ascending motion over the Maritime Continent, whereas dry, cold and descending anomaly over the central and the eastern Pacific. The location of MJO teleconnection patterns can be determined by seasonal mean upper-level zonal wind acted as a waveguide. The obvious change of the jet stream is found, especially over the eastern Pacific. Over this region, stationary Rossby wavenumber is expanded east and northward in the recent period than that in the past period. This change modifies the location and intensity of the teleconnection patterns based on the analysis of zonal wavenumber.

Based on the model experiments, the decadal change in the background states, especially zonal wind at the upper level, leads to strengthening the intensity of the MJO teleconnection pattern over the jet exit region but does not modify the pattern itself. On the other hand, the tropical heating modifies the teleconnection patterns over the North Pacific and North America, and these changes are similar to the observed difference maps between the two periods. Thus, the results indicate that the decadal change of the MJO teleconnection pattern is caused by the change of tropical diabatic heating rather than the change of zonal wind in the mid-latitude as background states. These changes are associated with the background states are changed into La Nina-like pattern in the recent period. This leads to moisture and SST increase over the warm pool region. In addition, the ascending motion of the vertical circulation in the background states strengthens over the eastern region of Maritime Continent, and then the convective anomaly becomes stronger over this region in the recent period than in the past period. It is thought that these background changes including the intensification of the vertical circulation lead to the enhancement of the MJO teleconnection pattern and its teleconnectivity over the upstream regions. Furthermore, there is close relationship of the MJO teleconnection patterns between P1 and El Nino years or P2 and La Nina years.

Contents

1. Introduction.....	1
1.1. Background and motivation.....	1
1.2. Objectives	10
2. Decadal change of the boreal winter MJO teleconnection since the mid-1990s.....	11
2.1. Background.....	11
2.2. Data and Methods	11
2.3. Observed decadal changes of the boreal winter MJO teleconnection pattern over the northern hemisphere.....	13
2.4. Decadal changes of factors influencing on the MJO teleconnection	18
2.4.1. Tropical diabatic heating related to MJO	18
2.4.2. Mean state of zonal wind in the middle latitudes	31
2.5. Summary.....	39
3. Contribution of tropical heating and mid-latitude mean state to decadal change of MJO teleconnection pattern	40
3.1. Background.....	40
3.2. Model experiment.....	40
3.2.1. Configuration.....	40
3.2.2. Verification of model experiments	41
3.3. Contribution of two factors to the decadal change of MJO teleconnection.....	49
3.3.1. Role of tropical heating and mid-latitude mean state in the decadal change of MJO teleconnection pattern.....	49
3.3.2. Effect of seasonal mean state on MJO teleconnection pattern	54
3.4. Relationship between decadal changes in tropical mean states and MJO teleconnection pattern	56
3.5. Summary.....	63
4. Conclusion	64
References.....	66

List of figures

Figure 1.1.1 Climatological composite map of OLR anomaly filtered with 20-100 days from 1980-2015 (36 years) for November-March for the eight phases. Red and blue colors indicate the convective and suppressed anomalies, respectively. The unit is $W m^{-2}$.

Figure 1.1.2 Frequency of occurrence for the MJO phase. The frequency is calculated in the number of strong MJO events at each MJO phase divided by the number of total strong MJO events. A strong MJO event is defined when amplitude in each MJO index is more than 1.0. Black and red bars indicate period 1 (P1, 1980-1994) and period 2 (P2, 1995-2009), respectively.

Figure 1.1.3 Regressed surface temperature (T_s) anomaly with 20-100 days filter onto OMI 1 (upper) and 2 (bottom). Results from left and right columns are calculated for boreal winter (Nov. -Mar.) during period 1 (P1, 1980-1996) and period 2 (P2, 1999-2015), respectively. The unit is $^{\circ}C$. The shaded region indicates statistical significance at the 99% confidence level.

Figure 1.1.4 Spatial patterns of OLR for (a) EOF1 on 15 Jan, (b) EOF2 on 15 Jan, (c) EOF1 on 15 Jul, and (d) EOF2 on 15 Jul. Arbitrary contour interval is $1W m^{-2}$. Blue shading corresponds to negative perturbations (Fig.2 from Kiladis et al., 2014).

Figure 1.1.5 Same as Figure 1.1.2 except for RMM index. For easy comparison, T_s anomalies from (a and b) and (c and d) are regressed onto -RMM2 and RMM1, respectively.

Figure 1.1.6 Spatial structures of EOFs 1 and 2 of the combined analysis of OLR (solid), u850 (dashed), and u200 (dotted) anomalies (Fig.1 from Wheeler and Hendon, 2004).

Figure 1.1.7 Pacific decadal oscillation (PDO) index. (Reference: <https://www.ncdc.noaa.gov/teleconnections/pdo/>)

Figure 2.3.1 Composite maps of OLR (shading) and GPH200 (contour, 10m interval) anomalies filtered with 20-100 days at all MJO phases during boreal winter for two periods, P1 (left column) and P2 (middle column). The right column indicates the difference of GPH200 anomaly between two periods, P2 and P1. Black dotted areas are exceeded statistical significance 99% level of 200 hPa geopotential height anomaly based on a two-tailed t-test. The units of OLR and geopotential height $W m^{-2}$ and m, respectively.

Figure 2.3.2 Teleconnectivity map at MJO phases 2, 3, 6, and 7 for two periods, P1 (left column) and P2 (right column). Teleconnectivity is calculated when MJO is a strong case (Amplitude ≥ 1.0). The solid black line is statistically significant with a two-tailed t-test with a 99% level.

Figure 2.3.3 Latitude-MJO phase plot of teleconnectivity at all MJO phases averaged over longitude 130E-60W for two periods, P1 (left column) and P2 (right column). Before the longitude average, teleconnectivity is calculated when MJO is an only strong case (Amplitude ≥ 1.0).

Figure 2.4.1 Variance of OLR anomaly over the warm pool region for two periods, P1 (top) and P2 (middle). Results are calculated by using (left) 20-100 days filtered OLR and (right) 20-100 days filtered OLR with zonal wavenumber 1-5. (bottom) The difference in OLR variance between P2 and P1. Black dotted areas are exceeded statistical significance level 99% of OLR variance based on F-test. The unit of OLR is $W^2 m^{-4}$.

Figure 2.4.2 Frequency of 20-100 days and zonal wavenumber 1-5 filtered negative OLR anomaly over the region where MJO propagates eastward. The frequency is calculated that the number of strong minimum (or minimum) points at each grid divided by the number of the total winter day. Only a strong OLR anomaly, which is stronger than a standard deviation of the OLR anomaly over 25S-15N, is considered. The numbers of strong MJO case in P1 and P2 are 1421 and 1215, respectively. The unit is 0.1 %.

Figure 2.4.3 Longitude -lag diagram of 20-100 days filtered (shading) and 20-100 days and zonal wavenumber 1-5 filtered (contour) OLR anomalies ($W m^{-2}$) for (a) P1 and (b) P2 regressed against a reference time series of the OLR anomaly by area-averaging over the central Pacific (160E-160W, 20S-10N). The anomalies are averaged over latitude 20S-10N. Shading regions indicate the statistical significance at the 1% level based on the two-tailed t-test.

Figure 2.4.4 Difference of the wintermean (a) SST (shading) and wind field at 850hPa (vector), (b) specific humidity at 850hPa, and (c) vertical structures of relative humidity (shading) and Walker circulation (contour) between P2 and P1. The units of SST, wind, specific humidity, relative humidity, and Walker circulation are $^{\circ}C$, $m s^{-1}$, $g kg^{-1}$, %, and $10^{11} kg s^{-1}$, respectively.

Figure 2.4.5 Spatial distribution of regressed specific humidity at 850hPa onto a reference time series of 20-100 days filtered OLR anomaly by area-averaging over the Indian Ocean (IO, 60-100E, 20S-15N) and the western Pacific (WP, 140-180E, 20S-15N) for P1 and P2.

Figure 2.4.6 Frequency of MJO occurrence at each MJO phase during P1 (black bar) and P2 (red bar) from (a) OMI and (b) RMM index. Only strong MJO cases are considered (Amplitude ≥ 1.0). One and two red stars signify significance statistically with 90% and 99% levels, respectively. The unit is %.

Figure 2.4.7 Density function of MJO amplitude based on OMI during boreal winter (November-March). The black and red lines indicate the past (P1) and recent (P2) periods. The difference between

two periods at all MJO phases shows a 99% level of statistical significance by the chi-square test. The unit is %.

Figure 2.4.8 Phase map of 20 – 100 days filtered OLR anomaly over the tropics for P1 (left) and P2 (right). Red and blue colors mean convective and suppressive anomalies, respectively. The unit is $W m^{-2}$.

Figure 2.4.8 (continue) Phase map of 20 – 100 days filtered OLR anomaly for P2 (contour) and difference of the filtered OLR anomaly between P2 and P1 (shading). Black dotted areas are exceeded the statistical significance level 99% of the filtered OLR anomaly based on a two-tailed t-test.

Figure 2.4.9 Winter-mean zonal wind at 200hPa for (a) P1 and (b) P2. (c) The difference of the zonal wind between P2 and P1. The shading region in (c) is exceeded the statistical significance level 99% of the filtered OLR anomaly based on a two-tailed t-test. The unit is $m s^{-1}$.

Figure 2.4.10 Stationary Rossby wavenumber (K_s) during the boreal winter for (a) P1 and (b) P2. In the a and b, the white regions indicate $\overline{u_m} < 0$. The regions where β_M is negative value are omitted and expressed as a white region. (c) The difference of K_s between two periods.

Figure 2.4.11 Zonal mean of the 20-100 days filtered GPH200 anomaly at 200hPa over the whole longitude with zonal wavenumber 0.

Figure 2.4.12 Zonal mean of intensity of the 20-100 days filtered GPH200 anomaly at 200hPa with zonal wavenumber 1 and 2. The intensity is defined as square root of square of the value averaged over whole longitude ($\sqrt{\overline{average(gph * gph, lon = 0, lon = 360)}}$).

Figure 3.2.1 Configuration of GFDL model.

Figure 3.2.2 Intensity of the GPH200 anomaly at the upper-level averaged over (a) East Asia (EA, longitude 90-160E and latitude 20-60N) and (b) North America (NA, longitude 160E-30W and latitude 20-80N) from Exp2. The intensity is defined as ($\sqrt{gph\ anomaly * gph\ anomaly}$).

Figure 3.2.3 MJO phase-mean MJO teleconnection patterns represented by the GPH anomaly at the upper-level from the observation (top) and the simulation from Exp1 (bottom). Results from the observation are the 20-100 days filtered GPH anomaly at 200hPa at lag 0 days, and from the model, simulation is GPH anomaly at 224.536hPa at lag ten days. The results are averaged over MJO phases 2 and 3, and 6 and 7.

Figure 3.2.4 Same as Figure 3.2.3 except for Exp2.

Figure 3.2.5 Spatial correlation coefficients between the model experiment, Exp1 and Exp2, and the observation. The coefficients are averaged over the northern hemisphere (longitude 0-360 and latitude 10-90N), and over the two phases, such as 2-3, 4-5, 6-7, and 8-1.

Figure 3.3.1 GPH200 anomalies at MJO phases 2 and 3 from the Exp1-4 (a-d) and its difference maps between Exp2 and Exp3 (d) and Exp3 and Exp1 (e). (f) is the difference map of the observed GPH200 anomaly between P2 and P1.

Figure 3.3.2 Same as Figure 3.3.1 except for MJO phases 6 and 7. Difference maps between Exp4 and Exp1 (d) and Exp2 and Exp4 (e).

Figure 3.3.3 Spatial correlation coefficients between the model experiments. The coefficients are averaged over the northern hemisphere (longitude 0-360 and latitude 10-90N) and over the two phases, such as 2-3, 4-5, 6-7, and 8-1.

Figure 3.3.4 GPH200 anomalies at MJO phases 2-3 and 6-7 from Exp2. The simulated results from (a-b) and (c-d) are obtained by using the wintertime and the summertime background states, respectively. The same wintertime tropical forcing is applied to all experiments.

Figure 3.4.1 Composite maps of OLR (shading) and GPH200 (contour, 10m interval) anomalies filtered with 20-100 days at MJO phase 3 during boreal winter for (a) P1, (b) P2, (c) El Nino years and (d) La Nina years for the whole period except 1996-1998, and (e) El Nino years and (d) La Nina years for the whole period including 1996-1998. The units of OLR and geopotential height $W m^{-2}$ and m, respectively.

Figure 3.4.2 Same as Figure 3.4.1 except for MJO phase 7.

Figure 3.4.3 Composite maps of OLR (shading) and GPH200 (contour, 10m interval) anomalies filtered with 20-100 days at all MJO phases during boreal winter for (left column) El Nino years and (right column) La Nina years for the whole period except 1996-1998.

Figure 3.4.4 Same as Figure 3.4.3 except for the whole period including 1996-1998.

Figure 3.4.5 Spatial correlation coefficients between the GPH200 anomalies obtained from the observation for P1, P2, El Nino and La Nina years. The correlation coefficients in (a) and (b) are obtained using El Nino and La Nina years for the whole period except and including 1996-1998, respectively. The coefficients are averaged over the northern hemisphere (longitude 0-360 and latitude 20-90N) at each MJO phase. Red- and blue-colored bars indicate the coefficients calculated with El Nino and La Nina years, respectively.

List of tables

Table 3.2.1 Information on model experiments

Chapter 1

1. Introduction

1.1. Background and motivation

Madden-Julian Oscillation (hereafter, MJO) is a dominant phenomenon over the tropics and characterized by a coupled system with anomalous deep convection and large-scale circulation. The convective system that could be described as outgoing longwave radiation (OLR) or rainfall initiates in Indian Ocean and propagates eastward through the Maritime Continent to the central Pacific with intraseasonal timescale shown in figure 1.1.1, which is generally 30-90 days and has a climatological MJO phase speed of about 5 m s^{-1} (Madden and Julian 1971, 1972). The MJO has two phases, active and inactive phases. These phases occur ahead of or behind each other. An active (inactive) phase that has the positive (negative) convective and rainfall anomaly with vertically upward (downward) motion combined with an anomalous convergence (divergence) and divergence (convergence) at lower- and upper-level, respectively.

The anomalous MJO-related convections generate the upper-level circulation anomalies, which are anticyclonic and cyclonic circulation behind and in front of anomalous convection, respectively, and these circulation anomalies propagate from the tropics or the subtropics to the middle or high latitudes. It is the stationary Rossby wave train and is generally called as teleconnection (Simmons 1982; Simmons et al. 1983; Lin et al. 2006).

Through this teleconnection, the MJO exerts numerous influences on weather and climate variability in the tropics and the extratropics (Matthews et al. 2004; Seo and Lee 2017). For instance, previous studies have explained that it affects the onset, development, and termination of El Niño–Southern Oscillation (ENSO; McPhaden 1999, 2004; Takayabu et al. 1999; Kessler and Kleeman 2000; Bergman et al. 2001; Zhang and Gottschalck 2002; Seo and Xue 2005), the American summer monsoons (Mo 2000; Higgins and Shi 2001; Jones and Carvalho 2002; Moon et al. 2013) and the active and break episodes of the Asian–Australian monsoon (Yasunari 1979; Lau and Chan 1986). The genesis and track of tropical cyclones are also affected by MJO in the eastern North Pacific (Maloney and Hartmann 2000), the northwest Pacific (Maloney and Hartmann 2001; Schreck and Molinari 2011; D. Kim et al. 2014), and the North Atlantic (Klotzbach 2010).

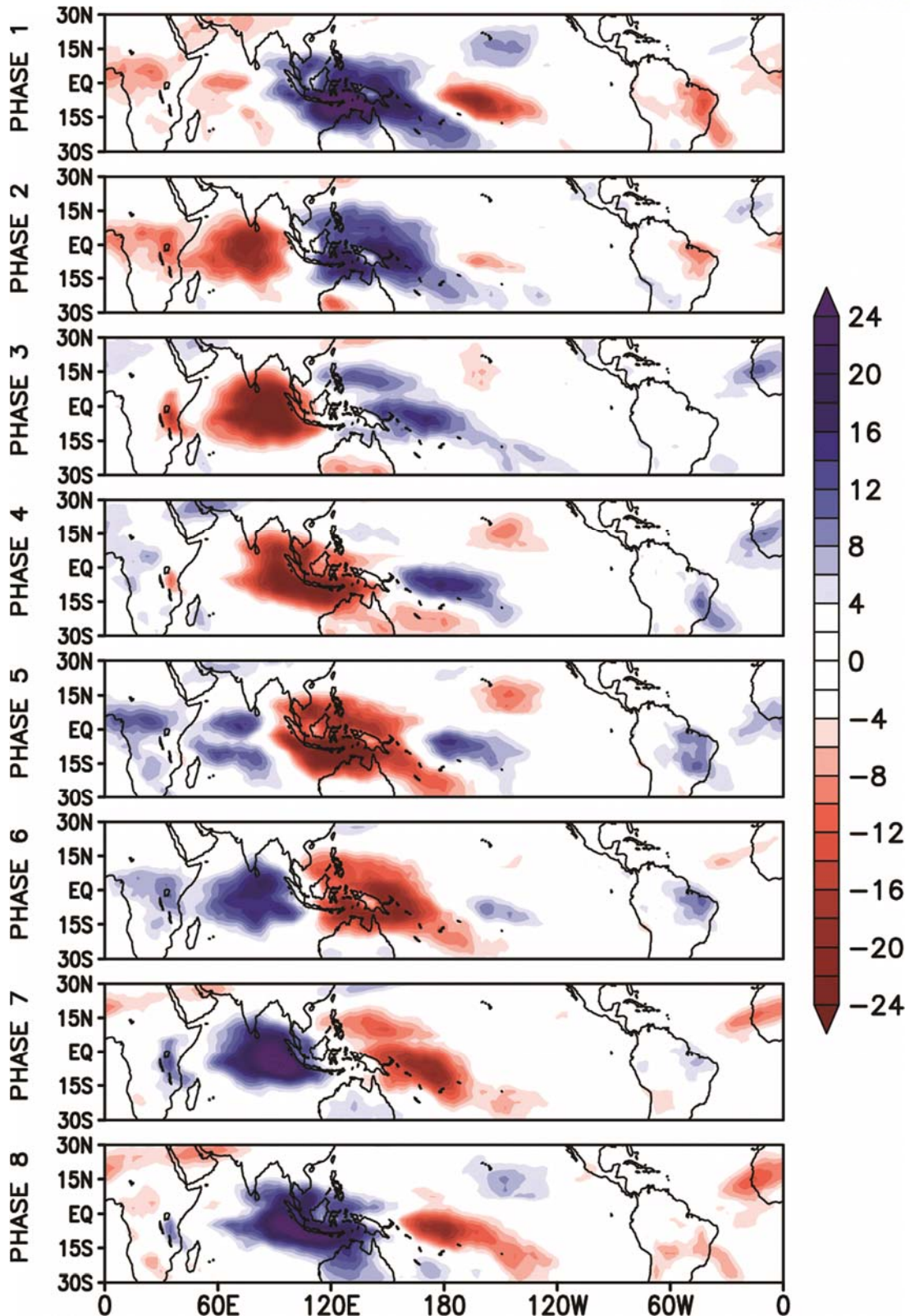


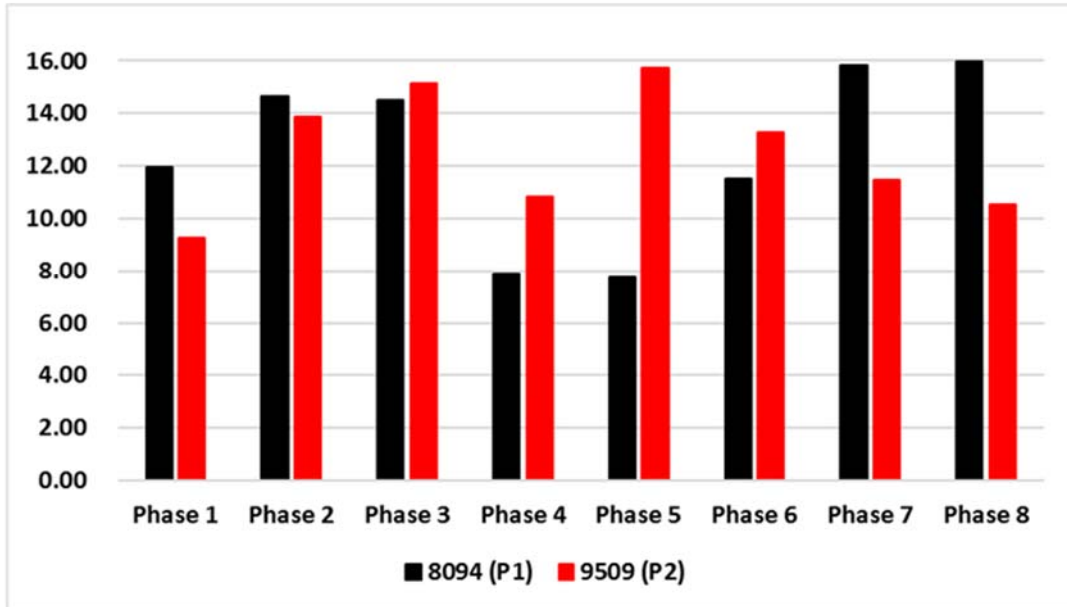
Figure 1.1.1 Climatological composite map of OLR anomaly filtered with 20-100 days from 1980-2015 (36 years) for November-March for the eight phases. Red and blue colors indicate the convective and suppressed anomalies, respectively. The unit is W m^{-2} .

Furthermore, by affecting the midlatitude weather via its teleconnection (Matthews et al. 2004; Seo and Lee 2017), the MJO is known as the dominant source of predictability in the intraseasonal time scale over the midlatitudes (Pegion and Kirtman 2008). For example, precipitation over North America (Matthews et al. 2004; Jones et al., 2011; Jones and Cavalho, 2012; Zhou et al. 2012; Baxter et al. 2014; Johnson et al. 2014, Barrett, 2018; Xiong et al., 2019), temperature over North America (Zhou et al., 2012; Rodney et al., 2013; Schreck III et al., 2013; Baxter et al., 2014; Yoo et al., 2015; Jenney et al., 2019), South America (Roundy 2014), precipitation over East Asia (Xiaolong et al., 2011; He et al., 2011; Jiao and Wu, 2019; Liu and Hsu, 2019), and surface air temperature over East Asia (Jeong et al. 2008; Jia et al. 2011; Lee et al., 2019) are known to be affected by the MJO's teleconnection.

The MJO teleconnection pattern is affected by various factors, including MJO activities. For instance, intensity and location (Jin and Hoskins 1995) and monopole or dipole patterns (Seo and Son 2012; Seo and Lee 2017) of the tropical convection anomaly, and background fields, such as subtropical jet stream or climatological upper-level zonal and meridional wind (Henderson et al. 2017; Kang and Tziperman, 2018a; 2018b). These factors have influenced not only interannual but also decadal variations. In particular, the MJO activities are changed by ENSO, which is one of the interannual variations, since it alters background fields such as sea surface temperature and upper- and lower-level wind. The circulation changes in the mean state are known to be important for wave propagation from the tropics to the midlatitudes. Thus, the pattern of MJO teleconnection is modified by the phase of ENSO. Moon et al. (2011) showed that the MJO teleconnection patterns during El Niño and La Niña years from 1979-2008 over extratropical regions differ distinctively even at the same MJO phase. These differences between ENSO phases are important because these may induce different even though the opposite effect over East Asia and North America.

According to many precedent studies, there is a long-term trend of MJO activity. Pohl and Matthews (2011) explained an increasing trend of annual-mean MJO amplitude from 1950 to 2005. In addition, the 11-year or 22-year running variance of MJO index calculated by using 30-96 days filtered zonal wind at 850 hPa with zonal wavenumber 1-3 averaged over latitude 5S-5N, and longitude 120E-180 shows similar result that there is increasing trend from 1950 to 2015 (Gushchina and Dewitte 2019) to the result from Pohl and Matthews (2011). Furthermore, Roxy et al. (2019) suggested that the Indo-Pacific warm pool shows a twofold expansion, and this changes the MJO life cycle. For example, the MJO phase duration over the Indian Ocean decreases by 3-4 days, but over Maritime Continent and the western Pacific increases by 5-6 days. This change influences global weather phenomena, precipitation due to an increase over the duration of the MJO phase from 5 to 7.

(a) RMM index



(b) OMI

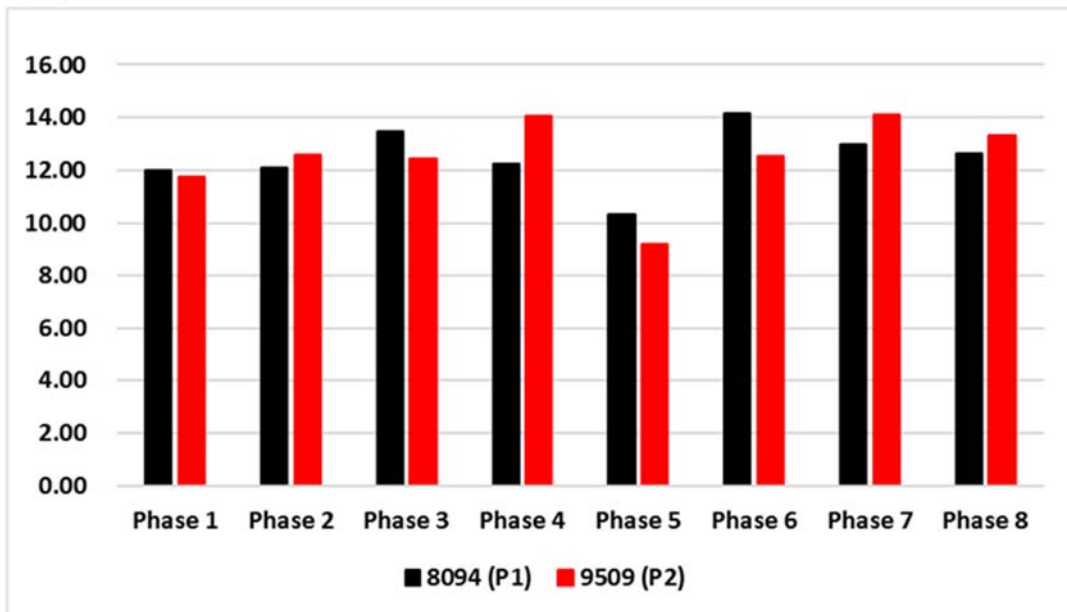


Figure 1.1.2 Frequency of occurrence for the MJO phase. The frequency is calculated in the number of strong MJO events at each MJO phase divided by the number of total strong MJO events. A strong MJO event is defined when amplitude in each MJO index is more than 1.0. Black and red bars indicate period 1 (P1, 1980-1994) and period 2 (P2, 1995-2009), respectively.

In addition, the frequency of strong MJO, which MJO amplitude is over 1.5, an occurrence is also changed from the former period (1979-1993) to the later period (1994-2008) during boreal winter (November to March) from Yoo et al. (2011). In the latter period, the frequency increases at MJO phases 4, 5, and 6, where the anomalous tropical convection is located over Maritime Continent and decreases over the Indian Ocean and the Western Pacific. This change in the MJO frequency influences on the Arctic warming that surface temperature anomaly filtered with 5-100 days increases over the Arctic during boreal winter in the latter period. Liu and Hsu (2019) also exhibited the change of MJO occurrence frequency during boreal winter (December to February). The number of MJO day increases and decreases during MJO phase 5-8 and 1-4, respectively, from Period 1 (1979-1994) to Period 2 (1995-2011), and this causes persistent heavy rainfall (PHR) during the winter over southern China (SC, latitude 21-26N and longitude 108-120E) decreases for Period 2 in comparison to Period 1.

It can be inferred that MJO activities had been changed according to climate change. The MJO teleconnection pattern and its influence on the weather all over the globe are also altered by these changes in the MJO activities. However, these previous studies that investigated the change in the occurrence of MJO phase used Real-time Multivariate MJO (RMM) index that OLR as a proxy for convection, and zonal wind at the upper (200hPa) and lower (850hPa) levels are combined to calculate and define the empirical orthogonal function (EOF). When the frequency change of MJO occurrence at each MJO phase is calculated using the OLR MJO index (OMI), the feature, which the number of MJO events during MJO phase 4-6 increases in the recent period (1995-2009) compared to the past period (1980-1994), is not dominant shown in figure 1.1.2. This result implies that the results from many previous studies might be dependent on the MJO index, such as RMM index or OMI, and the explanation for the decadal change of weather induced by MJO is insufficient based on the increase in the occurrence frequency of some MJO phases.

Then, we identify if weather phenomenon, such as surface temperature (T_s) with the intraseasonal variability induced by MJO is influenced by the type of the MJO index. Figure 1.1.3 shows the regressed spatial distribution of 20-100 days filtered T_s onto OMI 1 and 2 for boreal winter (November to March) during two periods, Period 1 (P1, 1980-1996) and Period 2 (P2, 1999-2015). Particularly, OMI 1 and 2 indicate MJO phase 2-3 (or 6-7) and phase 4-5 (or 8-1), respectively (Figure 1.1.4). There is a statistically significant change in the regressed T_s anomaly onto OMIs over the midlatitudes and the Arctic. The regressed T_s anomaly onto OMI 2 does not change distinctly over the Arctic, but it is found that the sign of the regressed T_s onto OMI 1 is changed between two periods. So, does this change also occur in the RMM index?

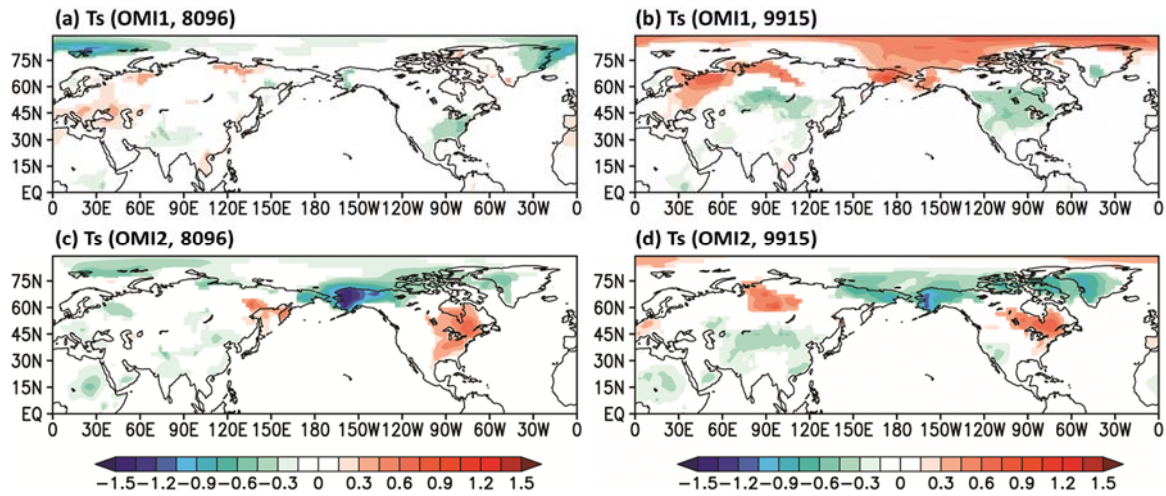


Figure 1.1.3 Regressed surface temperature (T_s) anomaly with 20-100 days filter onto OMI 1 (upper) and 2 (bottom). Results from left and right columns are calculated for boreal winter (Nov. -Mar.) during period 1 (P1, 1980-1996) and period 2 (P2, 1999-2015), respectively. The unit is $^{\circ}\text{C}$. The shaded region indicates statistical significance at the 99% confidence level.

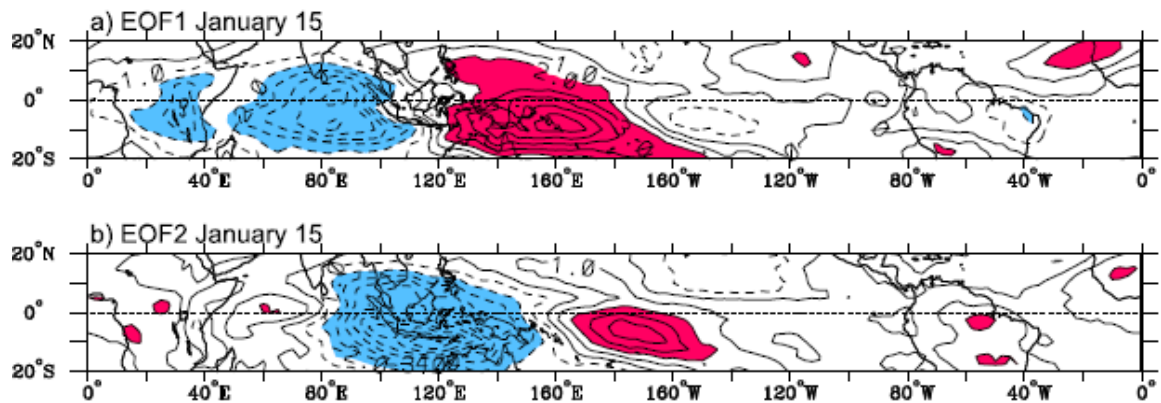


Figure 1.1.4 Spatial patterns of OLR for (a) EOF1 on 15 Jan, (b) EOF2 on 15 Jan, (c) EOF1 on 15 Jul, and (d) EOF2 on 15 Jul. Arbitrary contour interval is 1 W m^{-2} . Blue shading corresponds to negative perturbations (Fig.2 from Kiladis et al., 2014).

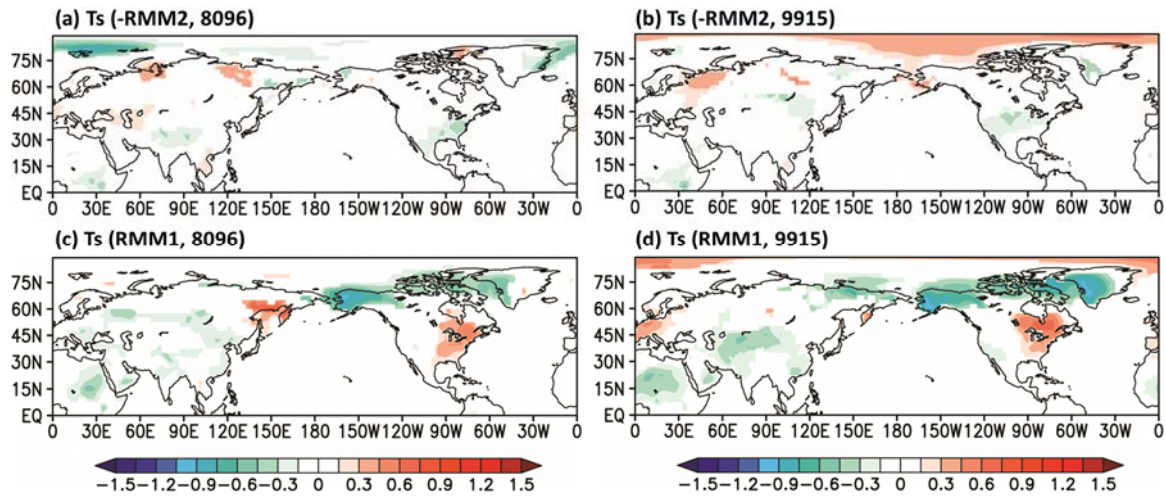


Figure 1.1.5 Same as Figure 1.1.2 except for RMM index. For easy comparison, Ts anomalies from (a and b) and (c and d) are regressed onto -RMM2 and RMM1, respectively.

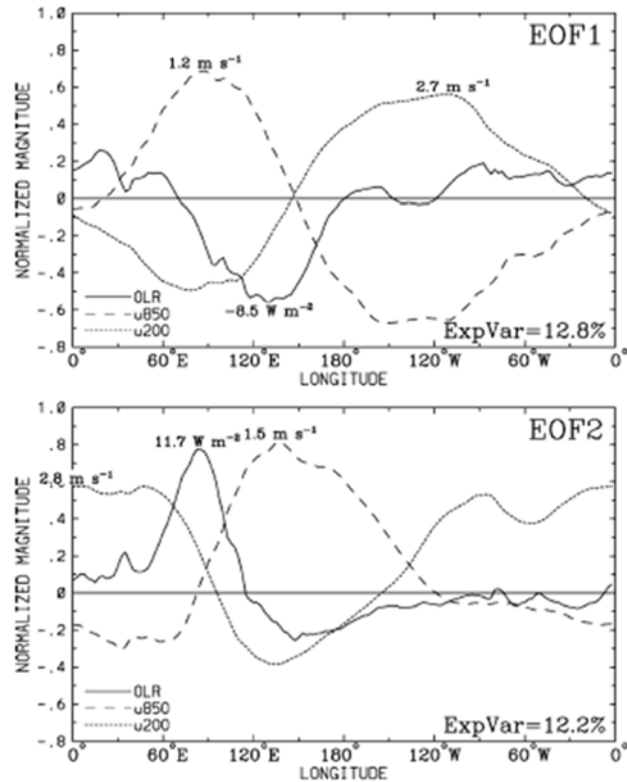


Figure 1.1.6 Spatial structures of EOFs 1 and 2 of the combined analysis of OLR (solid), u850 (dashed), and u200 (dotted) anomalies (Fig.1 from Wheeler and Hendon, 2004).

Figure 1.1.5 exhibits the regressed Ts anomalies filtered with 20-100 days onto RMM index. Especially, EOF 1 and 2 in RMM index denote different MJO phases of EOF 1 and 2 in OMI. That is, RMM 1 means MJO phase 4-5 (or 8-1), and RMM2 indicates MJO phase 6-7 (or 2-3) shown in figure 1.1.6. Thus, for easy comparison with the results from OMI, the Ts anomaly is regressed onto -RMM 2 and RMM1. This result is similar to the regressed Ts anomaly onto OMI, although the amplitude is smaller than the result from figure 1.1.3. These results can be interpreted that the decadal change of weather event between two periods is not influenced by type of the MJO index, and it is thought that this change is related to the MJO phases 2-3 or 6-7 that the anomalous convective system is located over the Indian Ocean and the western Pacific, not MJO phase 4-5 that the previous studies suggested an importance of the occurrence frequency of MJO phase 4-5.

The other factor affecting the MJO teleconnection pattern is the mean state of zonal wind at the upper troposphere, which is the subtropical jet stream (Hoskins and Ambrizzi 1993; Naoe et al. 1997; Naoe and Matsuda 1998; Branstator 2002; Kang and Tziperman 2018a; 2018b). There is a shift of phase of the pacific decadal oscillation (PDO) from positive to negative phase in 1998 shown in figure 1.1.7 (Bond et al. 2003; Mcphaden et al. 2011). Due to this regime shift, the spatial distribution of mean states, such as not only sea level pressure (SLP) and sea surface temperature (SST) but also atmospheric circulation at the upper- and lower-level. In addition, this is related to the increase in the frequency of central Pacific (CP) El Nino in the recent years. Therefore, the spatial distribution of mean SST shows the La Nina-like pattern in the recent period.

Thus, it is important to scrutinize whether there has been a decadal change in background states over the extratropics and MJO activities over the tropics during boreal winter and to understand how these changes influence on MJO teleconnection pattern to predict the change of MJO teleconnection pattern according to climate change such as the decadal variation. In this study, we investigate the influence of decadal change in background states over the extratropics and tropical forcing on the MJO teleconnection pattern and interpret the relationship between two factors and MJO teleconnection pattern using its dynamical mechanism.

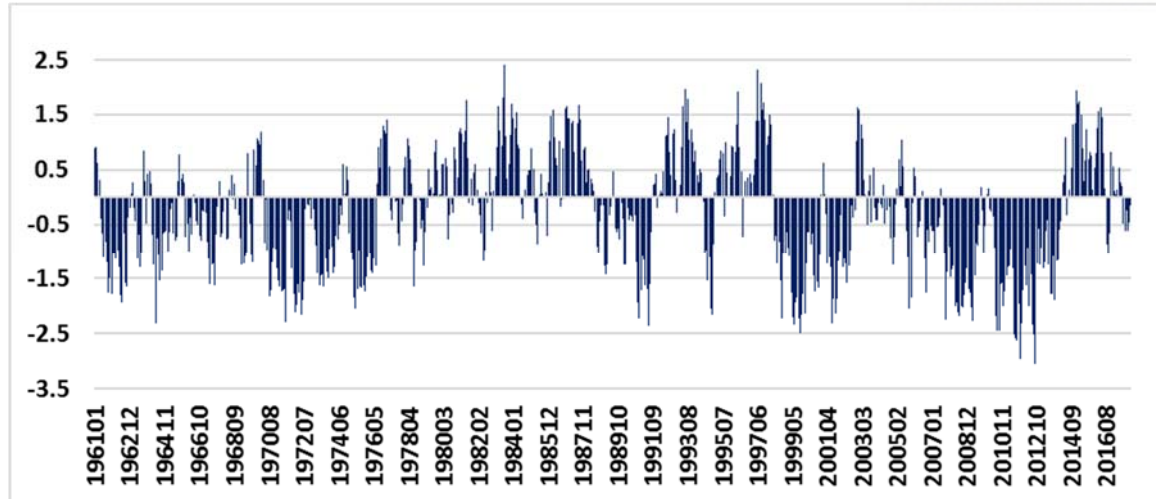


Figure 1.1.7 Pacific decadal oscillation (PDO) index. (Reference: <https://www.ncdc.noaa.gov/teleconnections/pdo/>)

1.2. Objectives

Based on previous studies, we have scientific questions,

- 1) Has the wintertime MJO teleconnection pattern changed with decadal variation?
- 2) How do the decadal changes of tropical MJO activity and background states in the midlatitude modulate the MJO teleconnection pattern?
- 3) Which factor is more important to the decadal change?

This study examines decadal changes of boreal wintertime MJO teleconnection pattern and two factors, tropical MJO activity as high-frequency climate variability and upper-level zonal wind in the background state over the extratropics as a low-frequency climate variability that modulate MJO teleconnection pattern by using observation data. And, the decadal change of the MJO teleconnection pattern resulted from the change of the factors is investigated by conducting GFDL dry dynamical core model experiments. Based on the experiments, the role of each factor in modulating the MJO teleconnection pattern and the relationship between the teleconnection pattern and the factors are interpreted dynamically.

Based on these scientific questions, this study is organized as followed. Chapter 2 explains the observed decadal changes of the boreal winter MJO teleconnection over the northern hemisphere and the decadal changes of factors influencing on the MJO teleconnection pattern. Chapter 3 shows the contribution of the factors to the decadal change of the MJO teleconnection pattern, especially the roles of and the relationship between the tropical diabatic heating and the mean state for the decadal change of MJO teleconnection are investigated. Chapter 4 summarizes the results, and future works are suggested in chapter 5.

Chapter 2

2. Decadal change of the boreal winter MJO teleconnection since the mid-1990s

2.1. Background

Diabatic heating and cooling anomalies over the tropics cause to upper- and lower-level circulation anomalies. Especially, the pattern of the upper-level circulation anomaly could be explained by linear stationary Rossby wave theory (Hoskins and Karoly 1981; Hoskins and Ambrizzi 1993). In that explanation, the Rossby wave source (Sardeshmukh and Hoskins 1988) associated with the MJO-related anomalous diabatic heating excites the Rossby waves, and the wave trains are formed following the group velocity of the Rossby waves.

In the intraseasonal timescale, the MJO activity over the tropics and the MJO teleconnection patterns over the extratropics are influenced by the mean states. However, the mean states, such as lower- and upper-level wind fields, SLP, SST over not only the tropics, but also the extratropics are changed since the mid-1990s that is called as the regime shift, and spatial patterns of these changes are similar to those in La Nina year. Furthermore, the MJO teleconnection pattern is also changed in a similar year (the mid-1990s).

Therefore, in this chapter, decadal changes in the MJO teleconnection pattern and the factors influencing on the MJO teleconnection pattern since the mid-1990s are investigated based on the analysis using the observation data, and the roles of these factors are organized based on the previous studies.

2.2. Data and Methods

Pacific decadal oscillation (PDO) is a prominent variation having decadal timescale over the Pacific basin and shows similar spatial distribution to El Nino/Southern Oscillation (ENSO). Positive (negative) PDO phase exhibits anomalous warm (cold) SST along the western coast of America over the North Pacific and El Nino (La Nina)-like SST distribution. This PDO index is obtained from the National Oceanic and Atmospheric Administration (NOAA) and used to examine the decadal change of the MJO

teleconnection pattern. Major changes in climate are observed in approximately 1976/1977 and 1997/1998 based on the PDO index (See Figure 1.1.7) or frequency of ENSO occurrence. PDO is changed from negative to a positive phase in about 1976/1977 and from positive to negative phase in about 1998/1999 (Bond et al. 2003). In addition, the central Pacific (CP) El Nino occurs more frequently after 1998/1999 than the eastern Pacific (EP) El Nino (McPhaden et al. 2011), and this result is consistent with the year when PDO phase is changed.

ERA-interim reanalysis daily data is used for vertical variables such as zonal and meridional wind, temperature, relative humidity, specific humidity, geopotential height, and omega, and has $1.5^\circ \times 1.5^\circ$ spatial resolution. Daily Advanced Very High-Resolution Radiometer (AVHRR) satellite data is also used for interpolated outgoing longwave radiation (OLR) and has $2.5^\circ \times 2.5^\circ$ spatial resolution. The Lanczos filter is applied with the 20-100 days period window to extract intraseasonal variability (ISV), and all data, including the filtered or the non-filtered data, are interpolated into $2.5^\circ \times 2.5^\circ$ resolution for the convenience.

The period adopted in this study is from 1980 to 2015 (36 years) due to the availability of AVHRR satellite data. The extended boreal winter (November to March) is only considered because MJO activity is strongest during the boreal winter. The year of regime shift is determined as 1998/1999, and based on this, the period is divided into two sub-period, the past period (P1, 1980-1996) and the recent periods (P2, 1999-2015) to inspect the decadal changes.

There are two MJO index, the Real-time Multivariate MJO (RMM) index and OLR-based on MJO index (OMI), which are commonly used. The RMM index is defined by Wheeler and Hendon (2004, hereafter WH04), who used the combined Empirical Orthogonal Function (EOF) analysis for OLR, and zonal wind at 850 hPa and 200 hPa. The OMI is defined by Kiladis et al. (2014) that is purely based on planetary-scale OLR anomaly with zonal wavenumber 1-3. This OMI index represents only convective activity without the effect of the adjacent circulation; thus, the OMI is used in this study to consider the only influence of the tropical convection on the upper-level circulation. The MJO amplitude and phase are defined as $(OMI1^2 + OMI2^2)^{1/2}$ and $\tan^{-1}(-OMI1/OMI2)$, respectively. Generally, strong and weak MJO cases have been defined as the MJO amplitude greater than and below 1.0, respectively. In the same manner, this study uses MJO amplitude 1.0 for a strong MJO case.

To obtain the anomaly fields with the intraseasonal timescale, the climatological fields of each variable are removed first, and the intraseasonal variability is derived by using 20-100 days filter with a Lanczos filter. MJO teleconnection pattern and tropical diabatic heating are expressed as geopotential height at 200 hPa and OLR anomalies and calculated using a composite method.

In this study, we try to find an occurrence location where the MJO-related OLR anomaly appears over the tropics. Thus, the following procedures are carried out.

- (1) The OLR anomalies are temporally and spatially filtered by 20-100 days filter and zonal wavenumber 1-5 filter and called as raw data (hereafter, raw).
- (2) Reference standard deviation (hereafter, std) is calculated for total P1 and P2 (1980-1996 and 1999-2015), not 1980-2015.
- (3) std and raw are averaged over latitude 25S-15N to reduce the noise value, and we only consider the OLR anomalies when latitude-averaged raw is more than latitude-averaged std to extract the distinct OLR anomaly.
- (4) Significant propagating anomalies are defined when the raw OLR anomalies from step 3 are more than std in the two-dimensional map.
- (5) Find the minimum (maximum) point of significant raw anomalies over a 2-d map. In this step, the minimum and maximum points denote the active and inactive phases, respectively.

2.3. Observed decadal changes of the boreal winter MJO teleconnection pattern over the northern hemisphere

Based on the year of regime shift, the decadal change of wintertime MJO teleconnection patterns at each MJO phase are examined and figure 2.3.1 displays the MJO teleconnection patterns for two periods and its difference. There are anticyclonic, and cyclonic circulation anomalies in west and east regions of the tropical convection anomaly located over the Indian Ocean and Maritime Continent addressed in Section 1. And, this anomalous upper-level circulation propagates from the central Pacific over the subtropics to North America or the North Atlantic. As the tropical OLR anomaly moves eastward from the Indian Ocean to the central Pacific, the MJO teleconnection pattern is shifted eastward, and the signs of the OLR and GPH200 anomalies are reversed. An interesting point in this figure is that the tropical OLR anomaly displays almost opposite signs between phases 1-4 and 5-8, where the OLR anomalies are located over the Indian Ocean and Maritime Continent, and the western and central Pacific, respectively, but signs of the MJO teleconnection patterns are not. This implies that the relationship between the tropical diabatic heating and its teleconnection pattern is not linear.

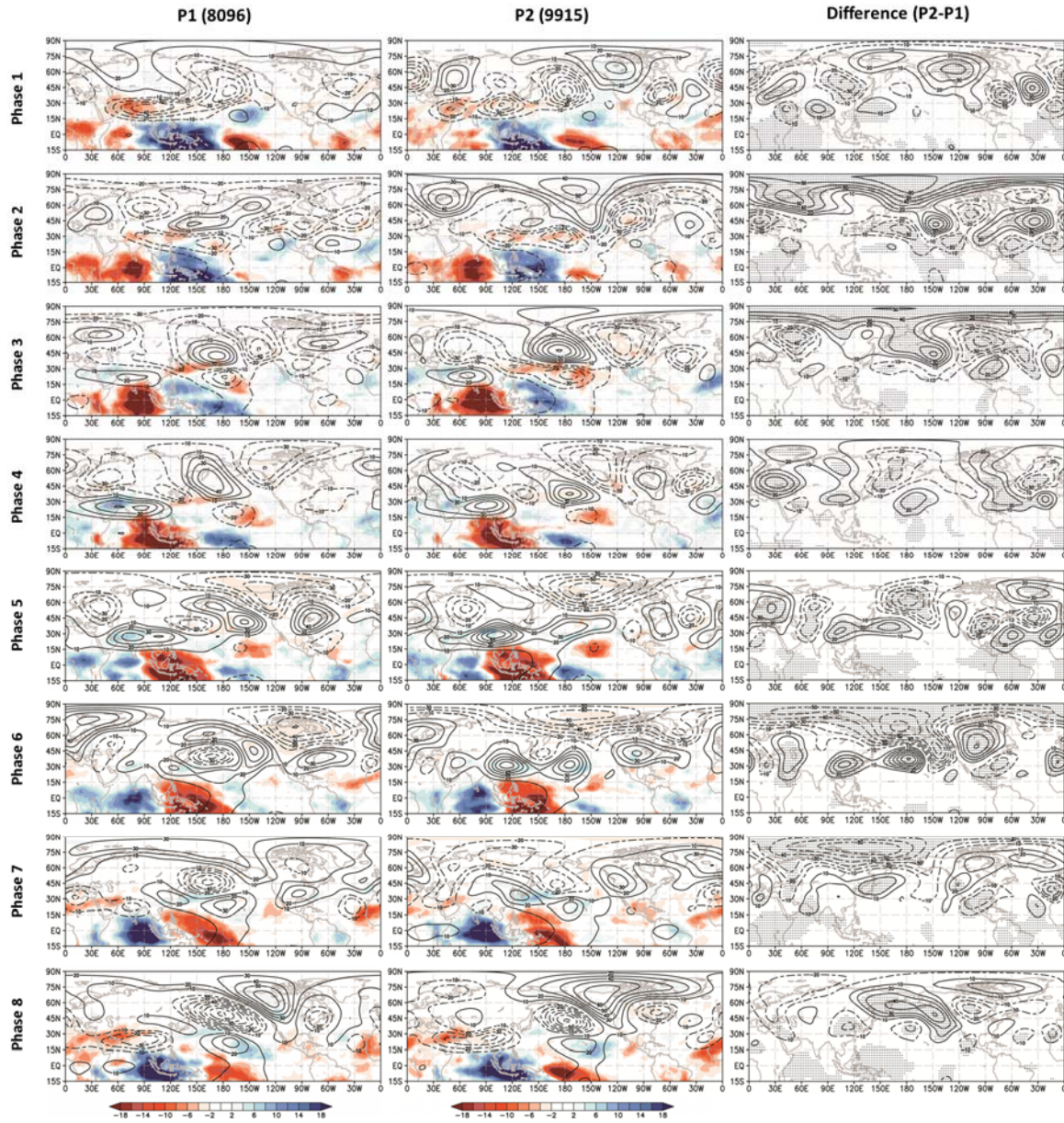


Figure 2.3.1 Composite maps of OLR (shading) and GPH200 (contour, 10m interval) anomalies filtered with 20-100 days at all MJO phases during boreal winter for two periods, P1 (left column) and P2 (middle column). The right column indicates the difference of GPH200 anomaly between two periods, P2 and P1. Black dotted areas are exceeded statistical significance 99% level of 200 hPa geopotential height anomaly based on a two-tailed t-test. The units of OLR and geopotential height m^{-2} and m, respectively.

Generally, the MJO teleconnection patterns are pronounced at MJO phases 3, 4, 7, and 8 in comparison to other MJO phases in common for two periods. In a comparison of the MJO teleconnection patterns at all MJO phases for P1, the MJO teleconnection patterns for P2 show that there are intensification and expansion of the upper-level circulation anomalies located over the North Pacific and North America where are the upstream region of the teleconnection pattern. In addition, the sign of the circulation anomaly over the north pole is changed, especially, MJO phase 2-3 and 6-7. For example, at MJO phases 2 and 3, the cyclonic circulation anomalies (a negative sign of the filtered GPH200 anomaly) are observed in P1, whereas there are anticyclonic circulation anomalies (the positive sign) in P2. In reverse, there are the anticyclonic and cyclonic circulation anomalies in P1 and P2, respectively, at MJO phases 6 and 7.

The difference of the MJO teleconnection patterns between two periods is distinct and statistically significant at all MJO phases that have statistical significance 99% level with a two-tailed t-test, not randomized. Particularly, the difference of the MJO teleconnection patterns is observed over the upstream region, and the difference over the north pole appears at only MJO phase 2, 3, 6 and 7 that the tropical convection anomaly has obvious dipole pattern, for example, the convective anomaly is located over the Indian Ocean or the western Pacific, but the suppressed anomaly is appeared over the western Pacific or the Indian Ocean, respectively, at the same time. Therefore, understanding which factors influence on the decadal change of the MJO teleconnection pattern is important to predict the MJO teleconnection pattern according to decadal change in future climate.

To compare a relationship between cells of the teleconnection pattern for the past and recent periods, “teleconnectivity” is considered (Wallace and Gutzler, 1981). This is a simple method of contrasting the strengths of teleconnection patterns for different grid points based on their respective one-point correlation maps.

$$T_i = | (r_{ij}) \text{ minimum for all } j | \quad \text{Equation. 2.3.1}$$

In Equation 2.3.1, r_{ij} indicates temporal correlation coefficients between the geopotential height anomalies at any selected grid point (denoted by the i subscript) and those at every other grid point in the hemisphere denoted by the j subscript, and T_i is termed the teleconnectivity of the i th grid point.

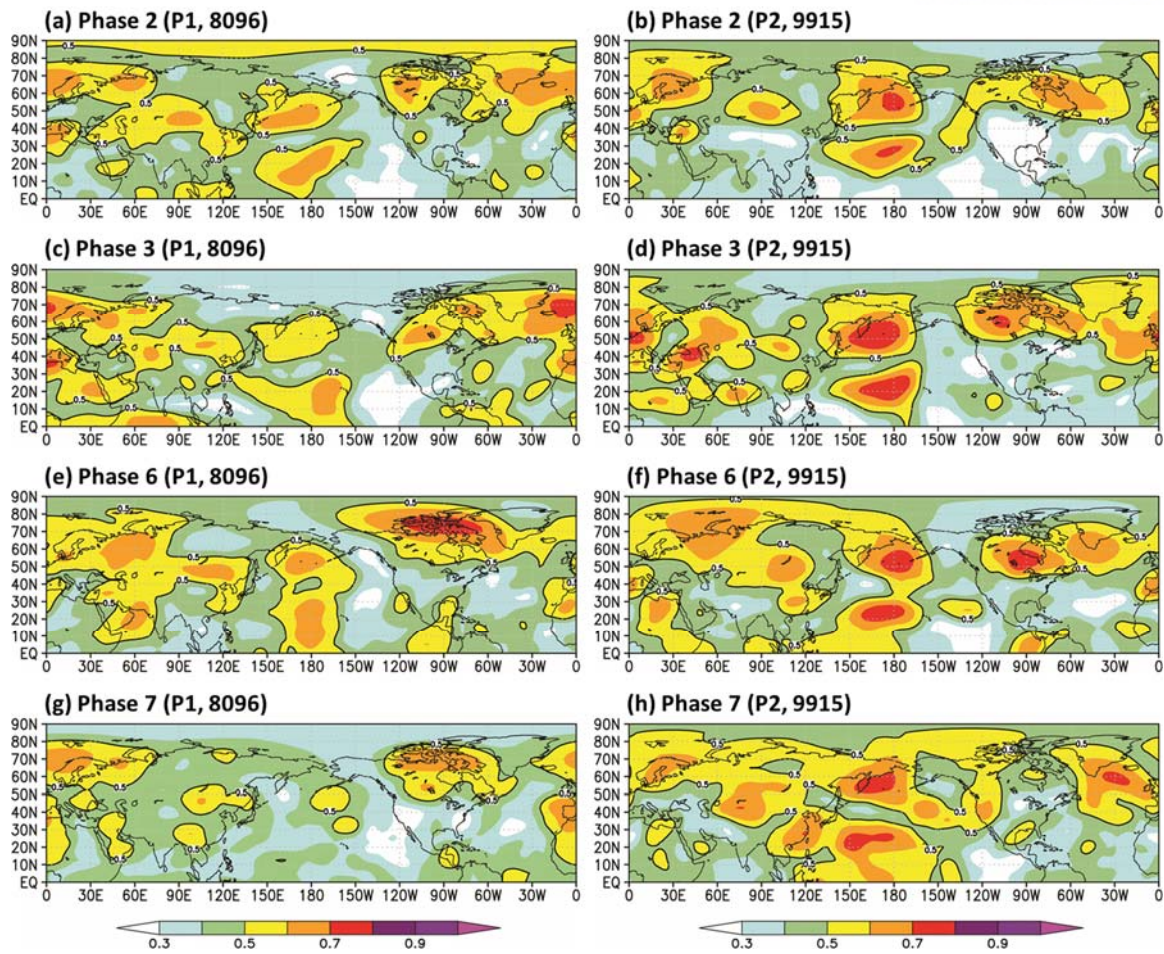


Figure 2.3.2 Teleconnectivity map at MJO phases 2, 3, 6, and 7 for two periods, P1 (left column) and P2 (right column). Teleconnectivity is calculated when MJO is a strong case (Amplitude ≥ 1.0). The solid black line is statistically significant with a two-tailed t-test with a 99% level.

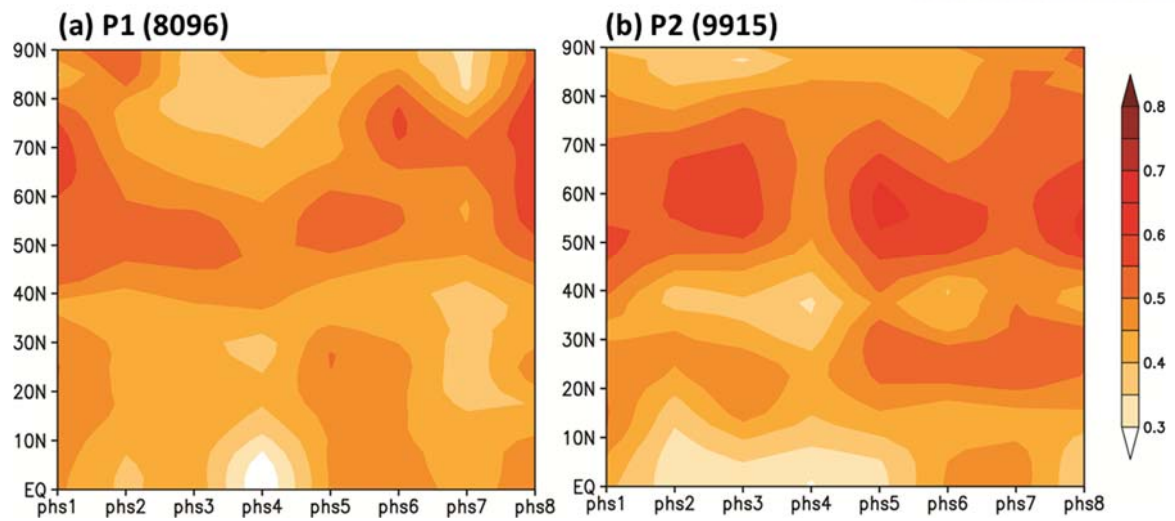


Figure 2.3.3 Latitude-MJO phase plot of teleconnectivity at all MJO phases averaged over longitude 130E-60W for two periods, P1 (left column) and P2 (right column). Before the longitude average, teleconnectivity is calculated when MJO is an only strong case (Amplitude ≥ 1.0).

Figure 2.3.2 shows spatial distributions of the teleconnectivity at MJO phases 2, 3, 6, and 7, in which the MJO phases display the clear difference of the teleconnection pattern over the north pole, for two periods, P1 and P2. The teleconnectivity in regions over North America, the North Atlantic, the Asian Continent, and the subtropics and the mid-latitude over the tropics are statistically more significant than in other regions for both periods. However, in the recent period, the teleconnectivity becomes much stronger, especially two cells over the Pacific where is the upstream region of the MJO teleconnection pattern than that for P1. Furthermore, the recent MJO teleconnectivity has become noticeably stronger in North America.

To summarize these features at all MJO phases, the result from figure 2.3.3 is obtained by calculating the teleconnectivity at all MJO phases averaged over longitude 130E-60W in the northern hemisphere for each period. The teleconnectivity between the subtropics and the mid-latitude tends to become strengthened, and this intensification is observed at most MJO phases in a higher latitude over 50N, although the teleconnectivity is rapidly weakened at MJO phase 4, and this is observed for both periods. These results imply that the intensity of the teleconnection pattern that is the teleconnectivity has increased, thereby increasing the relationship among the teleconnection cells over the upstream regions, particularly the Pacific and North America and the Atlantic.

2.4. Decadal changes of factors influencing on the MJO teleconnection

In this section, the decadal change of two factors, the tropical convection and the upper-level zonal wind over the extratropics as a background state, which influence on spatial distribution and intensity of MJO teleconnection pattern during boreal winter, are examined. We scrutinize how these factors could contribute to the MJO teleconnection pattern based on previous studies.

2.4.1. Tropical diabatic heating related to MJO

To identify the decadal change of the tropical diabatic heating, spatial distributions of the 20-100 days filtered OLR variance and the 20-100 days filtered OLR variance with zonal wavenumber 1-5 are compared over the warm pool region, and this is shown in figure 2.4.1. In the past period, the filtered OLR variance occurs evenly over the western and southern regions of Maritime Continent (longitude 80-140E) and the western Pacific (160E-180). In comparison, the result in P1, the filtered OLR variance in P2, is strengthened over the northern region of the Indian Ocean and near Maritime Continent and weakened over the southern region of the Indian Ocean and the western Pacific.

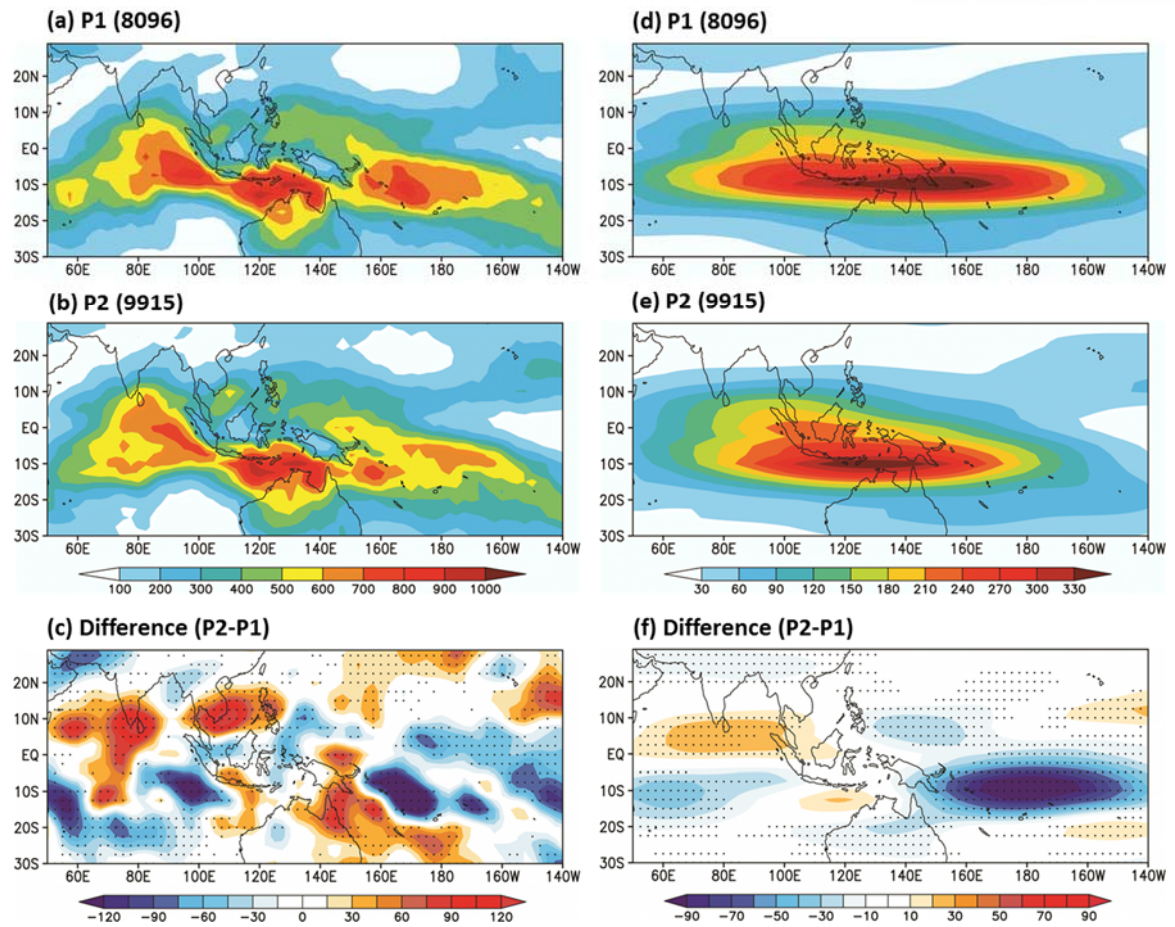


Figure 2.4.1 Variance of OLR anomaly over the warm pool region for two periods, P1 (top) and P2 (middle). Results are calculated by using (left) 20-100 days filtered OLR and (right) 20-100 days filtered OLR with zonal wavenumber 1-5. (bottom) The difference in OLR variance between P2 and P1. Black dotted areas are exceeded statistical significance level 99% of OLR variance based on F-test. The unit of OLR is $W^2 m^{-4}$.

This difference between two periods is also found in the variance of the filtered OLR with 20-100 days temporal filter and spatial filter of zonal wavenumber 1-5, which has characteristics of eastward propagation. The variance for P1 is zonally extended from the Indian Ocean to the central Pacific (longitude 80-170W) and is centered at the eastern region of Maritime Continent or the western Pacific. However, the variance for P2 is zonally shrunk (90-170E) and is centered at the southern region of Maritime Continent. This result provides that there is a clear decadal change over the warm pool region, especially the Indian Ocean, Maritime Continent, and the Pacific Ocean in the southern region of the equator.

The frequency of the MJO-related OLR anomaly is investigated for two periods to compare the location of the center of MJO activity. Figure 2.4.2 represents that the MJO in P1 appears mainly over the southern regions of the Indian Ocean, Maritime Continent, and the western Pacific. However, in P2, the main activity region is shrunk zonally. This means that the MJO-related OLR anomaly tends to not occur over the western Pacific in the recent period, and it is consistent with the result from figure 2.4.1.

Regressed 20-100 days filtered OLR anomaly averaged over latitude 20S-10N is shown in figure 2.4.3 to figure out the propagating feature of the OLR anomaly over the central Pacific. The results show that the regressed MJO-related OLR anomaly in P1 propagates over the eastern region of the dateline until lag 15 days, but that in P2 has difficulty in propagating to the central Pacific. This feature also explains the same results from figure 2.4.1. And 2.4.2.

So, why do these features appear? It is thought that these features, as explained above, are associated with the change of the background states. The difference in the background states between the two periods is represented in figure 2.4.4. Spatial distribution of the decadal changes in SST and low-level wind field resembles La Nina-like pattern; that is, there are warm and cold SST anomalies over the Indian Ocean and the western Pacific, and the central Pacific, respectively in the recent period. In addition, the easterly and westerly anomalies are dominant over the Pacific and the Indian Ocean, respectively. The spatial distribution of specific humidity anomaly at a low-level is consistent with the SST anomaly.

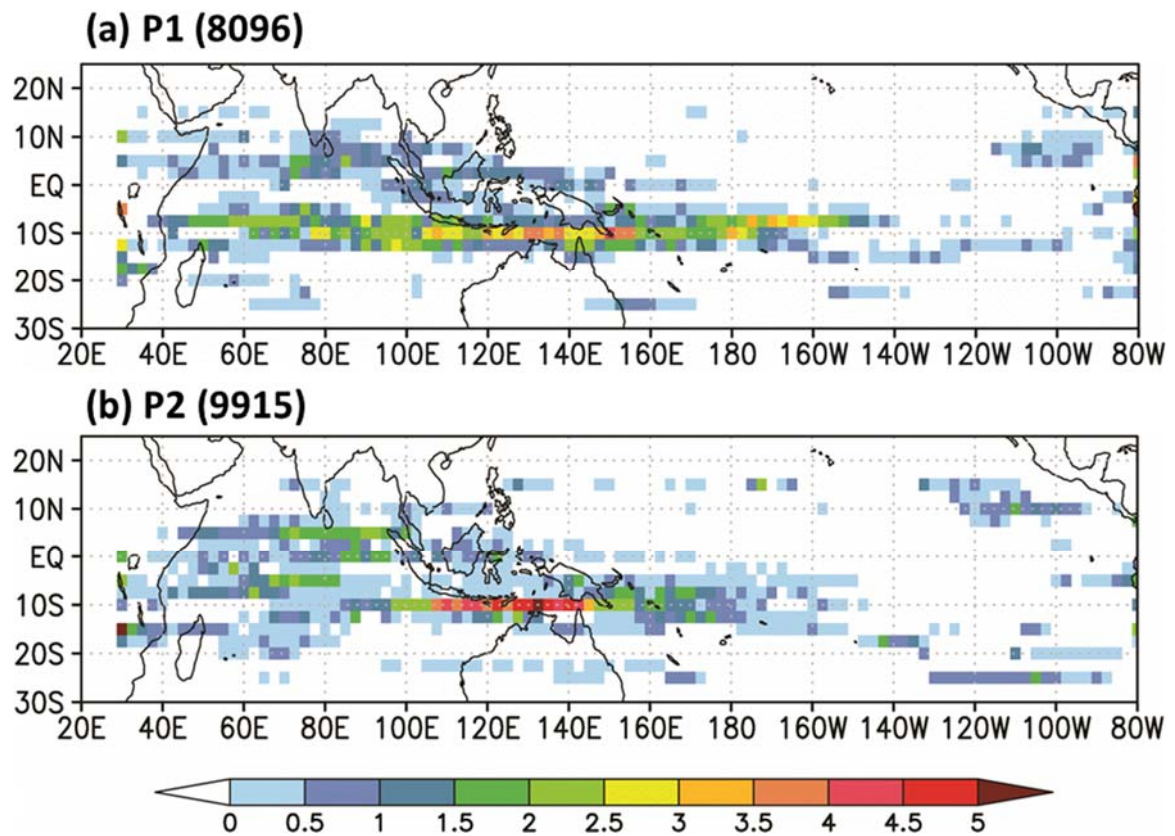


Figure 2.4.2 Frequency of 20-100 days and zonal wavenumber 1-5 filtered negative OLR anomaly over the region where MJO propagates eastward. The frequency is calculated that the number of strong minimum (or minimum) points at each grid divided by the number of the total winter day. Only a strong OLR anomaly, which is stronger than a standard deviation of the OLR anomaly over 25S-15N, is considered. The numbers of strong MJO case in P1 and P2 are 1421 and 1215, respectively. The unit is 0.1 %.

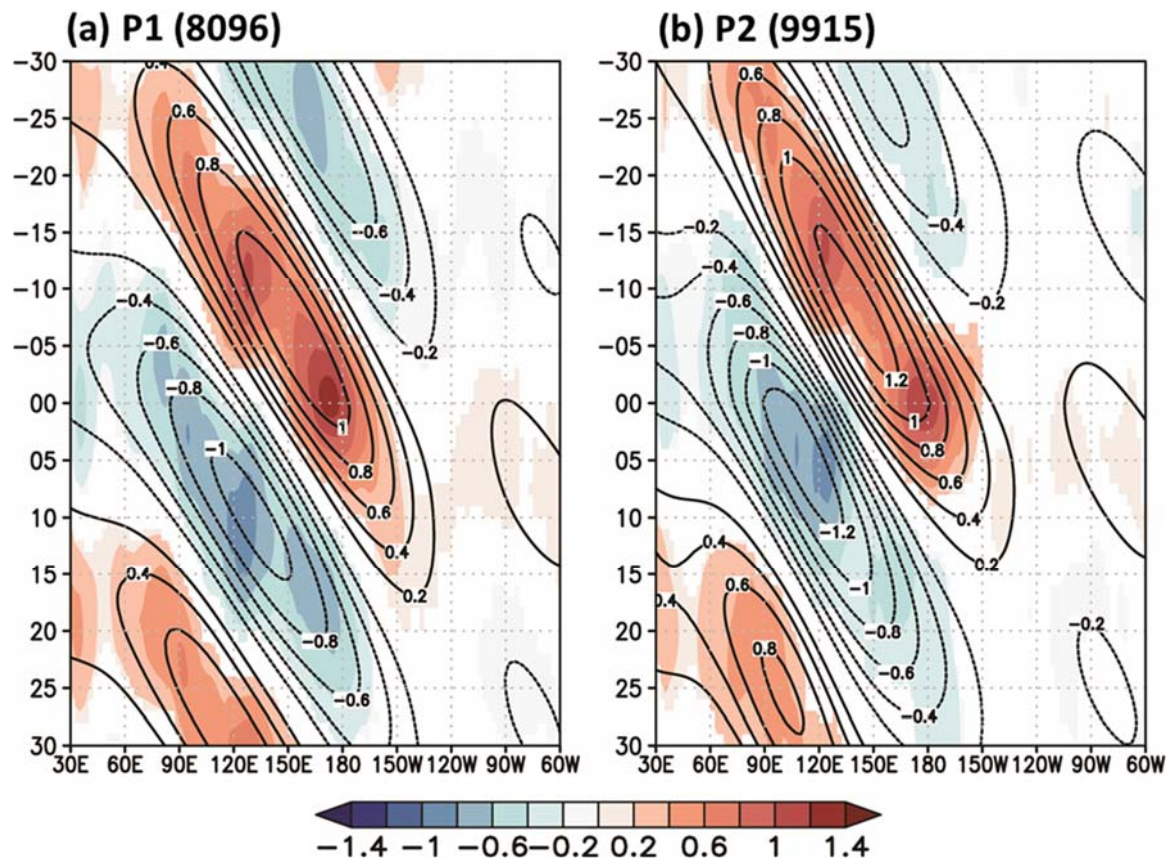


Figure 2.4.3 Longitude-lag diagram of 20-100 days filtered (shading) and 20-100 days and zonal wavenumber 1-5 filtered (contour) OLR anomalies (W m^{-2}) for (a) P1 and (b) P2 regressed against a reference time series of the OLR anomaly by area-averaging over the central Pacific (160E-160W, 20S-10N). The anomalies are averaged over latitude 20S-10N. Shading regions indicate the statistical significance at the 1% level based on the two-tailed t-test.

Difference of vertical structures of relative humidity and Walker circulation display that there are dry and wet anomalies over the central Pacific and Maritime Continent, respectively, and ascending (descending) motion appears over Maritime Continent (the central and eastern Pacific), which is the same location with warm SST and wet specific humidity at 850hPa anomalies. This result suggests that background states are clearly changed between two periods and are also associated with La Nina-like distribution.

Then, the relationship between the changes of the wintertime background states and the MJO-related OLR anomaly over the tropics is investigated. In particular, the regression analysis is performed using specific humidity at 850hPa in the mean field over two regions, the Indian Ocean (IO) and the western Pacific (WP), where the difference of the frequency of MJO-related OLR anomaly is obvious between two periods. The result from figure 2.4.5 explains that the tropical OLR anomaly is influenced by the low-level moisture field, especially, a decrease of the frequency over WP is associated closely with the decrease of the specific humidity at low-level in the recent period.

As described in Chapter 1, RMM index and OMI are calculated in different ways, and with different variables, for instance, RMM index uses OLR and 200hPa and 850hPa zonal wind, but OMI uses only OLR. Because of this, these two indices express the MJO-related OLR anomaly over the tropics and the MJO activity differently. For example, the frequencies of strong MJO cases from OMI and RMM index are different (Figure 2.4.6). In the case of OMI, there is the little decadal change in the frequency between two periods, but the frequency decreases at MJO phase 6, where the convective anomaly is located over the western Pacific. This denotes that OMI does not tend to describe the decrease of the MJO activity over the central Pacific. However, in the case of RMM index, the frequency of MJO occurrence represents a distinct difference between two periods. The frequency increases at MJO phase 4, 5, and 6 where the anomalous convection is located over Maritime Continent and the western Pacific in the recent period., whereas decreases at other MJO phases (1, 2, 3, 7, and 8) where the convective anomaly is located over the Indian Ocean or the central Pacific. This result is consistent with Yoo et al. (2011). Especially, there is a statistically significant difference with 90% and 99% levels at only MJO phases 4 and 5, respectively, where the anomalous tropical convection is located over the Maritime Continent based on RMM index.

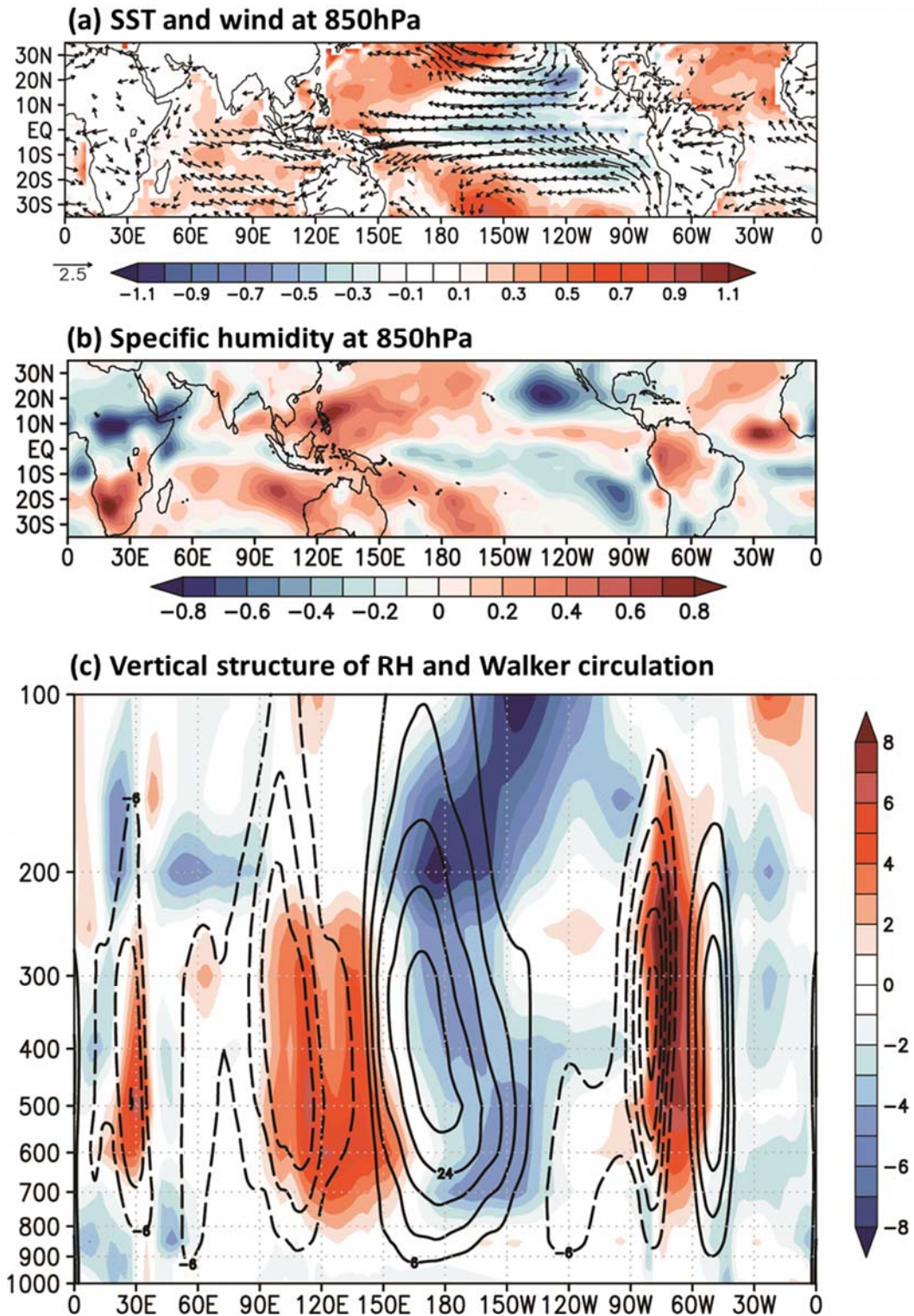


Figure 2.4.4 Difference of the wintermean (a) SST (shading) and wind field at 850hP (vector), (b) specific humidity at 850hPa, and (c) vertical structures of relative humidity (shading) and Walker circulation (contour) between P2 and P1. The units of SST, wind, specific humidity, relative humidity, and Walker circulation are $^{\circ}\text{C}$, m s^{-1} , g kg^{-1} , %, and $10^{11} \text{ kg s}^{-1}$, respectively.

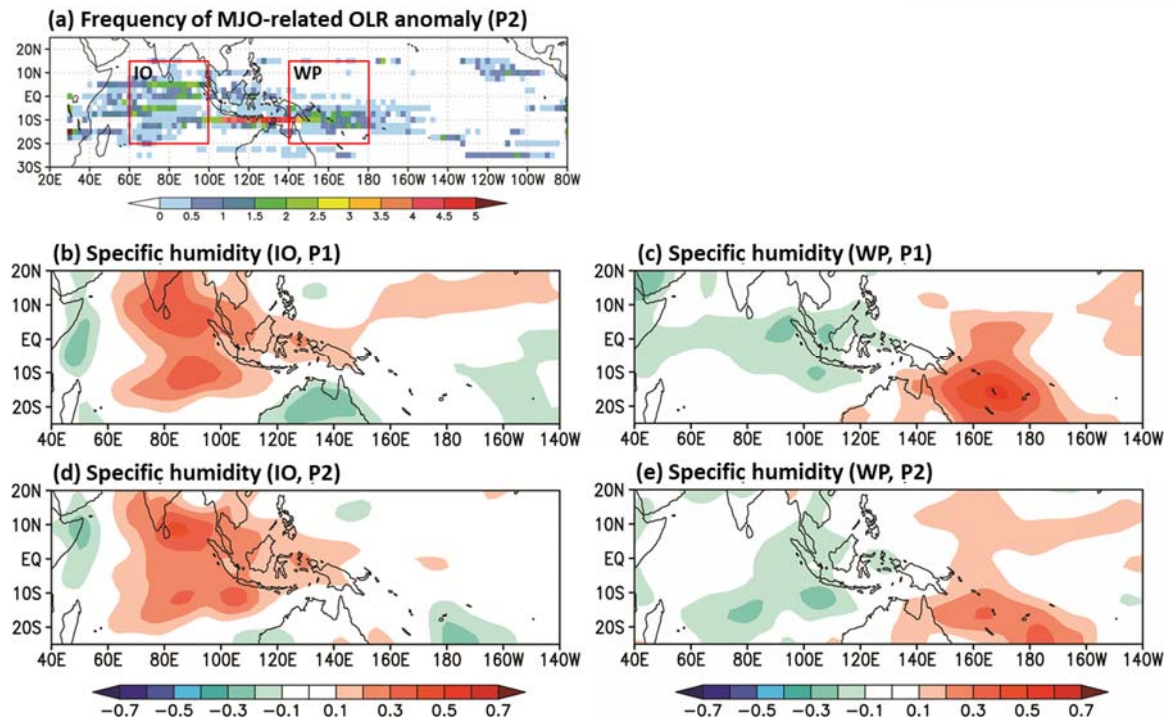
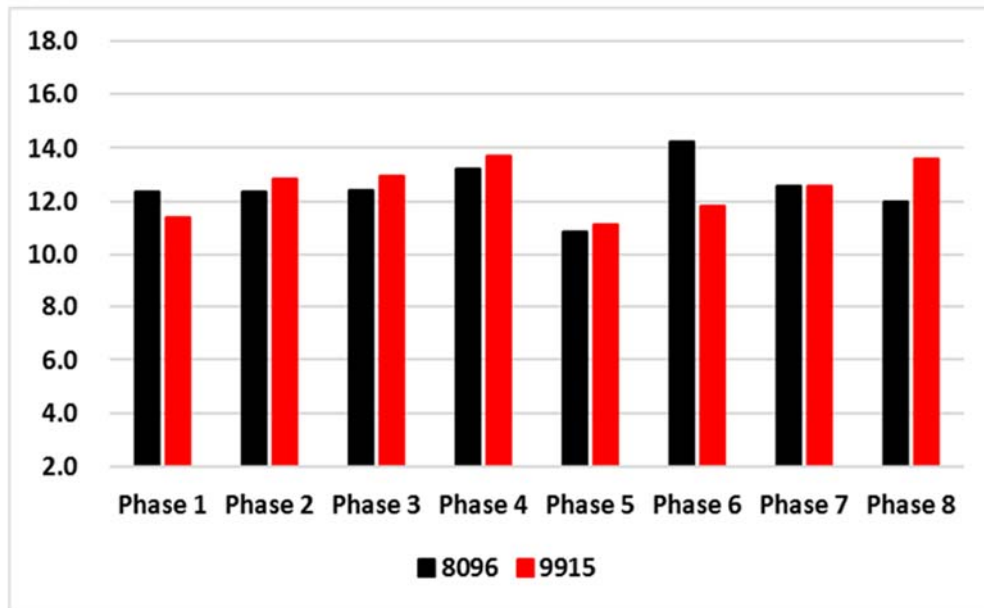


Figure 2.4.5 Spatial distribution of regressed specific humidity at 850hPa onto a reference time series of 20-100 days filtered OLR anomaly by area-averaging over the Indian Ocean (IO, 60-100E, 20S-15N) and the western Pacific (WP, 140-180E, 20S-15N) for P1 and P2.

(a) OMI



(b) RMM index

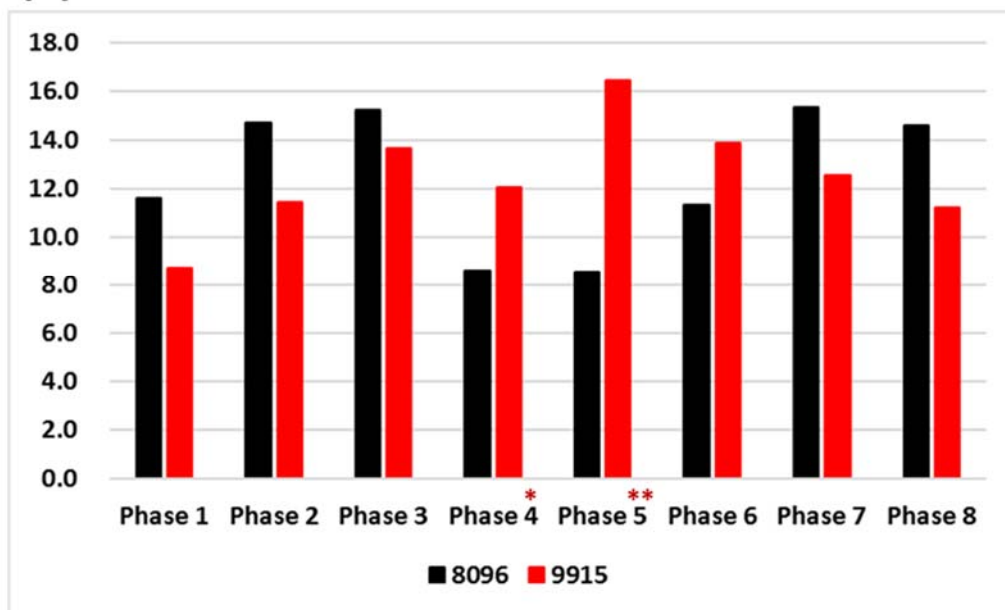


Figure 2.4.6 Frequency of MJO occurrence at each MJO phase during P1 (black bar) and P2 (red bar) from (a) OMI and (b) RMM index. Only strong MJO cases are considered (Amplitude ≥ 1.0). One and two red stars signify significance statistically with 90% and 99% levels, respectively. The unit is %.

As the previous result compared the change in frequency of the MJO occurrence in each phase, figure 2.4.7 compares the MJO amplitude between two periods. Most phases depict the peak near the approximately amplitude 0.8-1.2, and the ratio of strong MJO case with the amplitude of more than 1.0 accounts for approximately 70 percent of the total cases. The interesting point is that density function of the MJO amplitude based on OMI shows a decrease in MJO amplitude over the western Pacific and the increase over Maritime Continent, and these difference at all MJO phases represent 99% level of statistical significance by the chi-square test, which is a simple and common goodness-of-fit test. Moreover, these changes, particularly MJO phase 4-5 and 6-7, are coherent with the decadal change of background states and the variance of the filtered OLR anomalies shown in figure 2.4.4 and 2.4.1, respectively.

Figure 2.4.8 (a)-(b) describes MJO phase maps of 20-100 days filtered OLR anomaly over the tropics for P1 and P2. At MJO phase 1 to 3, where the negative anomaly of OLR is located over the Indian Ocean, the intensity of the negative OLR anomaly is stronger in P2 than that in P1 but is weaker in P2 than that in P1 at MJO phase 4 to 8. This difference in the intensity between two periods is well described in figure 2.4.8-c. The phase map of the difference of the filtered OLR anomaly exhibits that both the convective and suppressive anomalies are significantly changed from P1 to P2, and the dominant difference is found over the Maritime Continent and western Pacific. The location of the OLR anomaly is changed, and the anomaly in the recent period tends to be concentrated near the Maritime Continent, and these changes are statistically significant with significance level 99%. It is thought that this is associated with La Nina-like change of mean states over the tropics.

In summary, the decadal change of background states over the tropics leads to the change of MJO activity over the tropics, such as occurrence frequency, variance, and spatial distribution of anomalous convection and suppression, and this will affect the change of MJO teleconnection pattern.

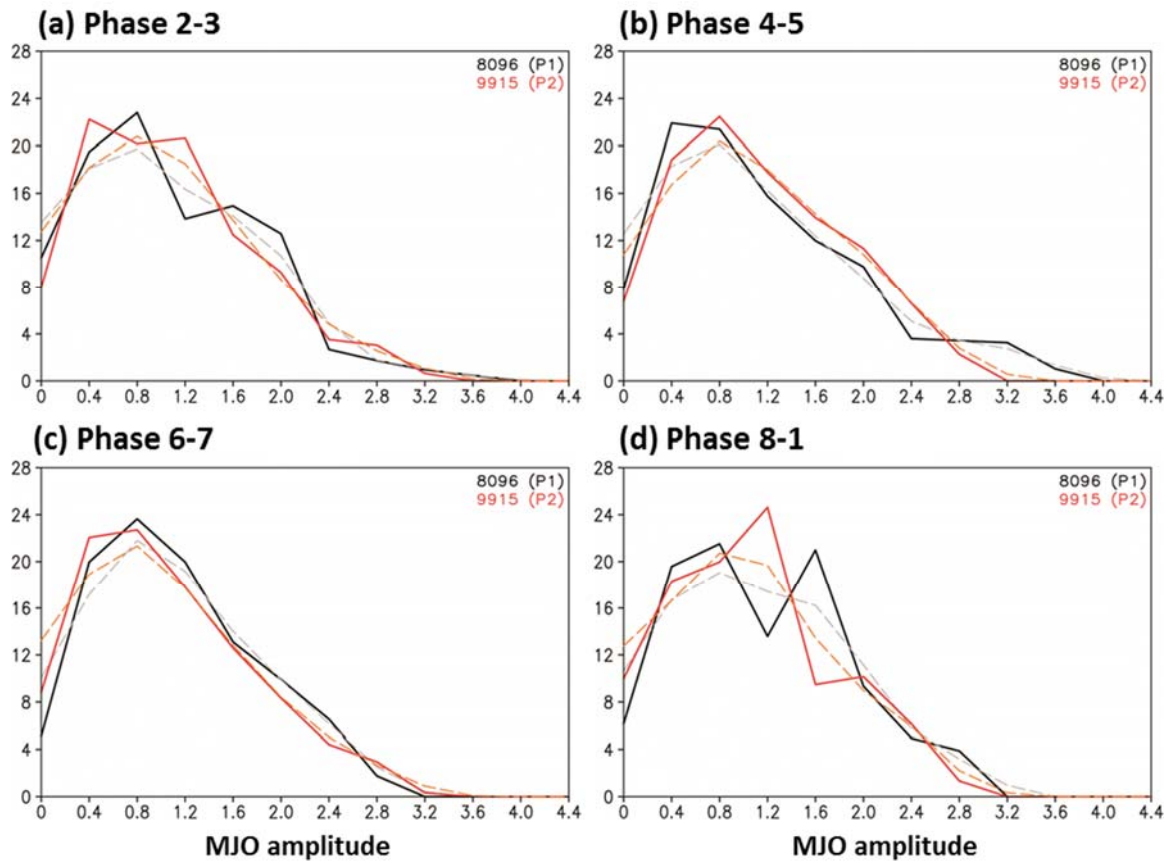


Figure 2.4.7 Density function of MJO amplitude based on OMI during boreal winter (November-March). The black and red lines indicate the past (P1) and recent (P2) periods. The difference between two periods at all MJO phases shows a 99% level of statistical significance by the chi-square test. The unit is %.

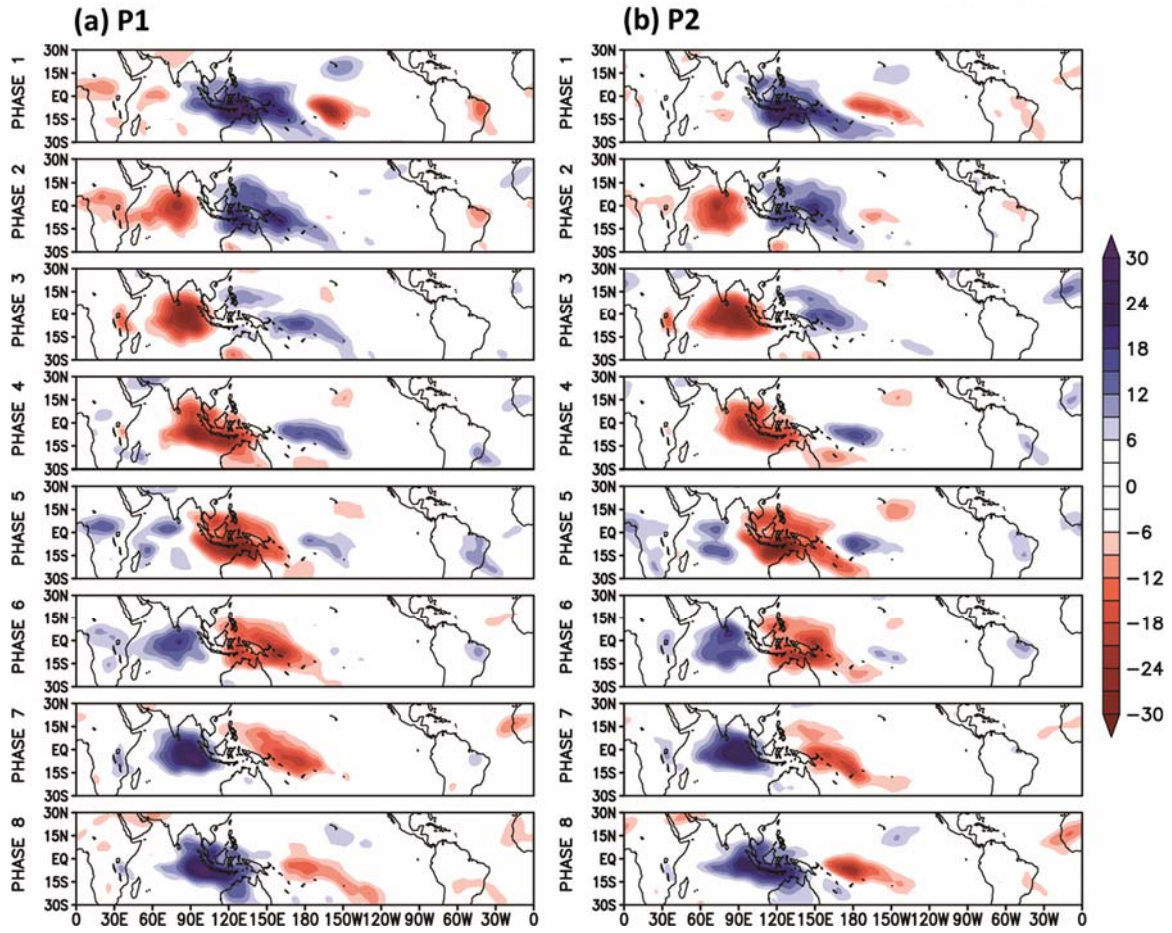


Figure 2.4.8 Phase map of 20 – 100 days filtered OLR anomaly over the tropics for P1 (left) and P2 (right). Red and blue colors mean convective and suppressive anomalies, respectively. The unit is W m^{-2} .

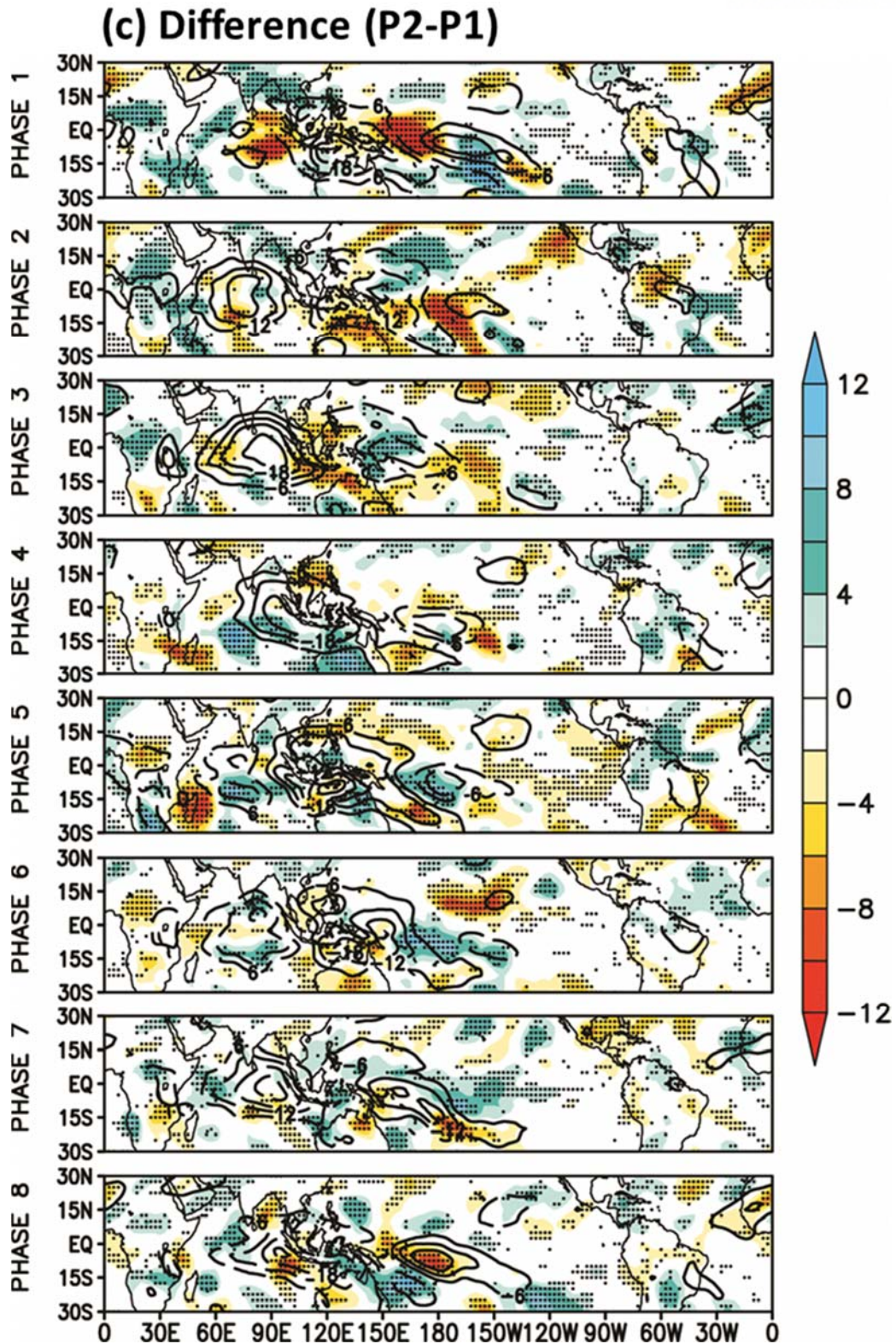


Figure 2.4.8 (continue) Phase map of 20 – 100 days filtered OLR anomaly for P2 (contour) and difference of the filtered OLR anomaly between P2 and P1 (shading). Black dotted areas are exceeded the statistical significance level 99% of the filtered OLR anomaly based on a two-tailed t-test.

2.4.2. Mean state of zonal wind in the middle latitudes

Based on the Rossby wave dynamics, stationary Rossby wavenumber is determined using the time-mean or the seasonal-mean upper-level zonal wind as a background state and acts as a waveguide of Rossby wave propagation (Hoskins and Ambrizzi, 1993). In additions, many previous studies, such as Simmons (1982), Wester and Holton (1982), Branstator (1983), Naoe et al. (1997; 1998), and Kang and Tziperman (2019), explained the impact of longitudinal variation of zonally asymmetric zonal wind at upper-level as a mean state. This denotes that the subtropical and its variation in both the subtropics and the mid-latitude are important to determine the location of the MJO teleconnection pattern during the boreal winter.

The seasonal-mean zonal wind at 200hPa for two periods are compared, and its decadal change is examined in figure 2.4.9. The wintertime upper-level zonal wind in P1 is located over latitude 20-40N and penetrates through the Pacific and reaches the Atlantic without a halt, although the wind is weakened over the eastern Pacific, the zonal wind in P2 ceases over the eastern Pacific reversely. There is an obvious difference in the wintertime zonal wind over some regions. In particular, the zonal wind in the recent period is weakened at about latitude 30N and strengthened at about latitude 10N and 50N over the eastern Pacific and strengthened in latitude 30-40N over East Asia.

Stationary Rossby wavenumber (K_s) is analyzed to examine the impact of the decadal change of these upper-level zonal wind on the decadal change of Rossby wave propagation. K_s is obtained through the following equation 2.4.1-4 (Hoskins and Ambrizzi, 1993; Freitas and Rao, 2011; Henderson et al. 2017), and is calculated by using the time-mean, in this study, seasonal (winter)-mean upper-level (200hPa) zonal wind.

$$\omega = Uk - \frac{\beta^* k}{K_s^2} \quad \text{Equation 2.4.1}$$

ω : the frequency of the Rossby wave

U : the zonal velocity of the background state

k : the zonal wavenumber

l : the meridional wavenumber

K_s : $\sqrt{k^2 + l^2}$ (the total wavenumber)

$\beta^* = \frac{\partial f}{\partial y} - \frac{\partial^2 U}{\partial y^2} = \beta - U_{yy}$ (meridional gradient of the absolute vorticity)

$$Ks = \sqrt{\frac{a\beta_M}{\bar{u}}} \quad \text{Equation 2.4.2}$$

$$\bar{u} = \frac{\bar{U}}{a\cos\theta} \quad \text{Equation 2.4.3}$$

$$\beta_M = \frac{2\Omega\cos^2\theta}{a} - \frac{\partial}{\partial y} \left[\frac{1}{\cos^2\theta} \frac{\partial}{\partial y} (\bar{u}_m * \cos^2\theta) \right] \quad \text{Equation 2.4.4}$$

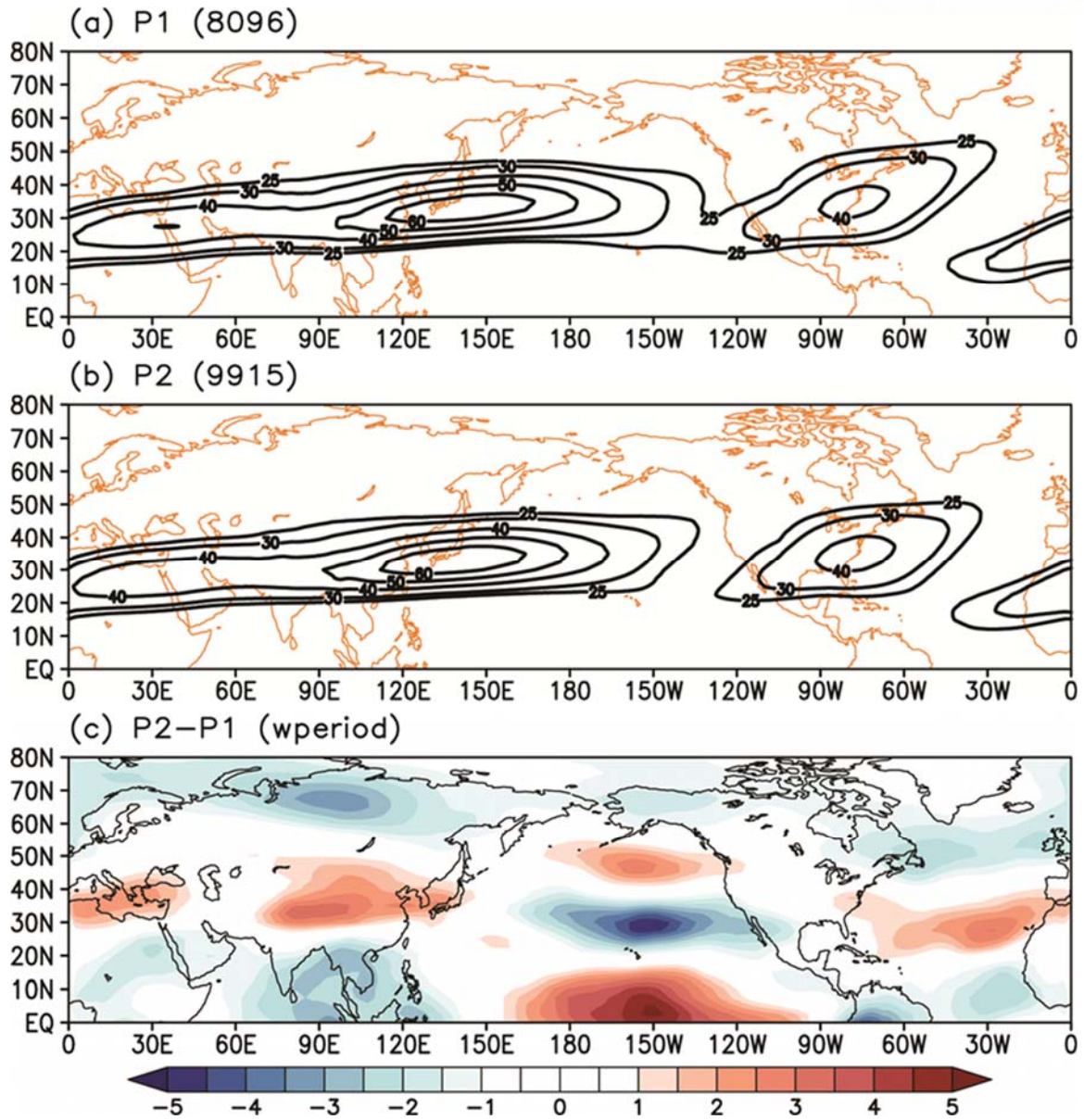


Figure 2.4.9 Winter-mean zonal wind at 200hPa for (a) P1 and (b) P2. (c) The difference of the zonal wind between P2 and P1. The shading region in (c) is exceeded the statistical significance level 99% of the filtered OLR anomaly based on a two-tailed t-test. The unit is m s^{-1} .

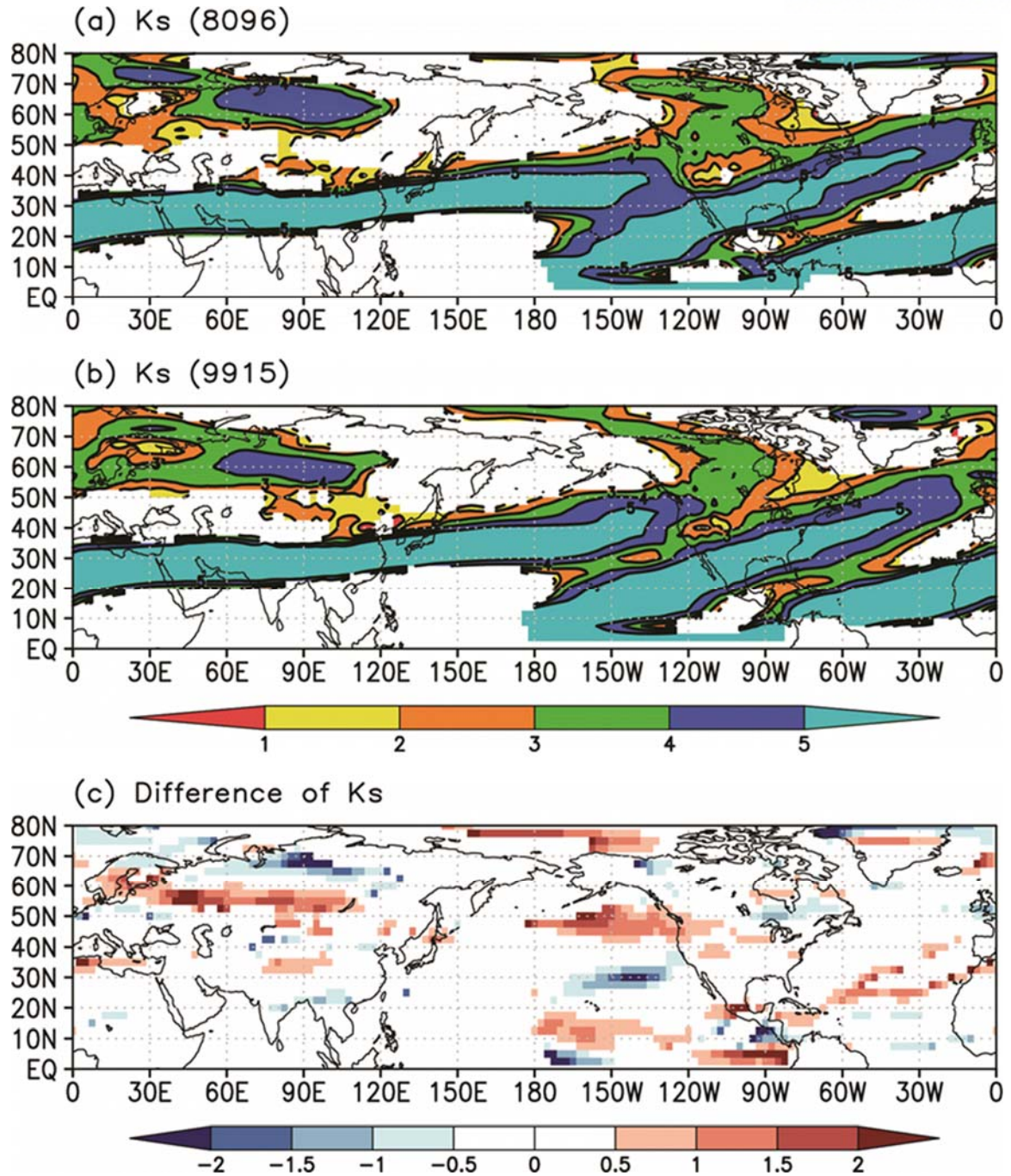


Figure 2.4.10 Stationary Rossby wavenumber (K_s) during the boreal winter for (a) P1 and (b) P2. In the a and b, the white regions indicate $\overline{u_m} < 0$. The regions where β_M is negative value are omitted and expressed as a white region. (c) The difference of K_s between two periods.

Figure 2.4.10 represents the stationary Rossby wavenumber during the boreal winter for two periods, and the difference between them. Spatial distributions of the Ks are similar to each other; however, there is a clear difference when the regions, such as the eastern Pacific and North America, are focused. In the recent period, the Ks is expanded east and northward over the eastern Pacific and penetrated North America, particularly Ks is more than 4. Moreover, Ks between 2 and 4 reaches near the Chukchi Sea at the Arctic, and it is considered that the decadal change in Ks could affect the decadal change of the surface temperature associated with MJO phase 2-3 or 6-7 over the Arctic as delineated in figure 1.1.4 and 1.1.5. The spatial distribution of the difference in figure 2.4.10-c resembles the difference of wintertime zonal wind at 200hPa in figure 2.4.9-c. Therefore, it can be thought that it is related to the decadal change of the wintertime zonal wind at the 200hPa because the recent zonal wind becomes stronger over the same region, as shown in figure 2.4.9.

The relationship between the GPH200 anomaly filtered with 20-100 days as MJO teleconnection pattern and Ks is compared at MJO phases 3, 4, 7, and 8. In a comparison of P1, the MJO teleconnection pattern is clearly shifted eastward and expanded over the northern Pacific and North America, where are the upstream region, according to the east and northward, expanded Ks during these four MJO phases. However, these relationships are not identified at all MJO phases; for example, the relationships are not recognized at the MJO phases 5 and 6.

Based on the linearized Rossby wave dispersion relationship, the upper-level zonal wind as a background state plays an important role in determining the zonal and meridional wavenumber (Equation 2.4.1-4). Therefore, the decadal change of the upper-level zonal wind will modify the zonal and meridional wavenumbers of Rossby wave, even though the spatial distribution of the MJO teleconnection patterns.

Figure 2.4.11 describes latitude-MJO phase plots of the zonal-mean GPH200 anomaly filtered with 20-100 days with zonal wavenumber 0. There is a distinct change in signs of the circulation anomalies at MJO phase 2-3 and phase 6-7 at the Arctic, although the signs are not changed over the mid-latitude near 30N that there are positive and negative sign changes at MJO phase 4-6 and 8-2, respectively. For instance, in the recent period, the sign of the circulation anomaly in the Arctic changed from negative (positive) to positive (negative) at MJO phase 2-3 (6-7). Furthermore, zonal wavenumber 1 and 2 also changed, as shown in figure 2.4.12. In the case of zonal wavenumber 1, the MJO teleconnection patterns appear robustly over latitude 10-20N and 30-40N, and the teleconnection pattern is vigorous in only MJO phase 5 and 6 in regions above latitude 60N for P1. However, in the recent period, the MJO teleconnection pattern develops and propagates from the subtropics to the higher latitudes compared to the past period. Furthermore, unlike the result from P1, the MJO teleconnection patterns are intensified at only two latitudinal bands, such as 20-30N and 60-80N in the recent period. The MJO teleconnection

patterns with zonal wavenumber 2 for both periods appear intensively in the mid-latitudes, and the difference of the intensity of the MJO teleconnection patterns between two periods is caused according to the MJO phases rather than the latitudinal bands. For instance, in the recent period, the teleconnection pattern tends to be stronger at MJO phase 1-3 and weaker at MJO phase 4-8 than the past period.

In summary, the decadal change of the subtropical jet stream or upper-level zonal wind during the boreal winter leads to the change in the stationary wavenumber of the MJO teleconnection pattern, and this can induce the spatial distribution of the teleconnection pattern. Especially, this change is obviously observed at the mid-latitude and the Arctic.

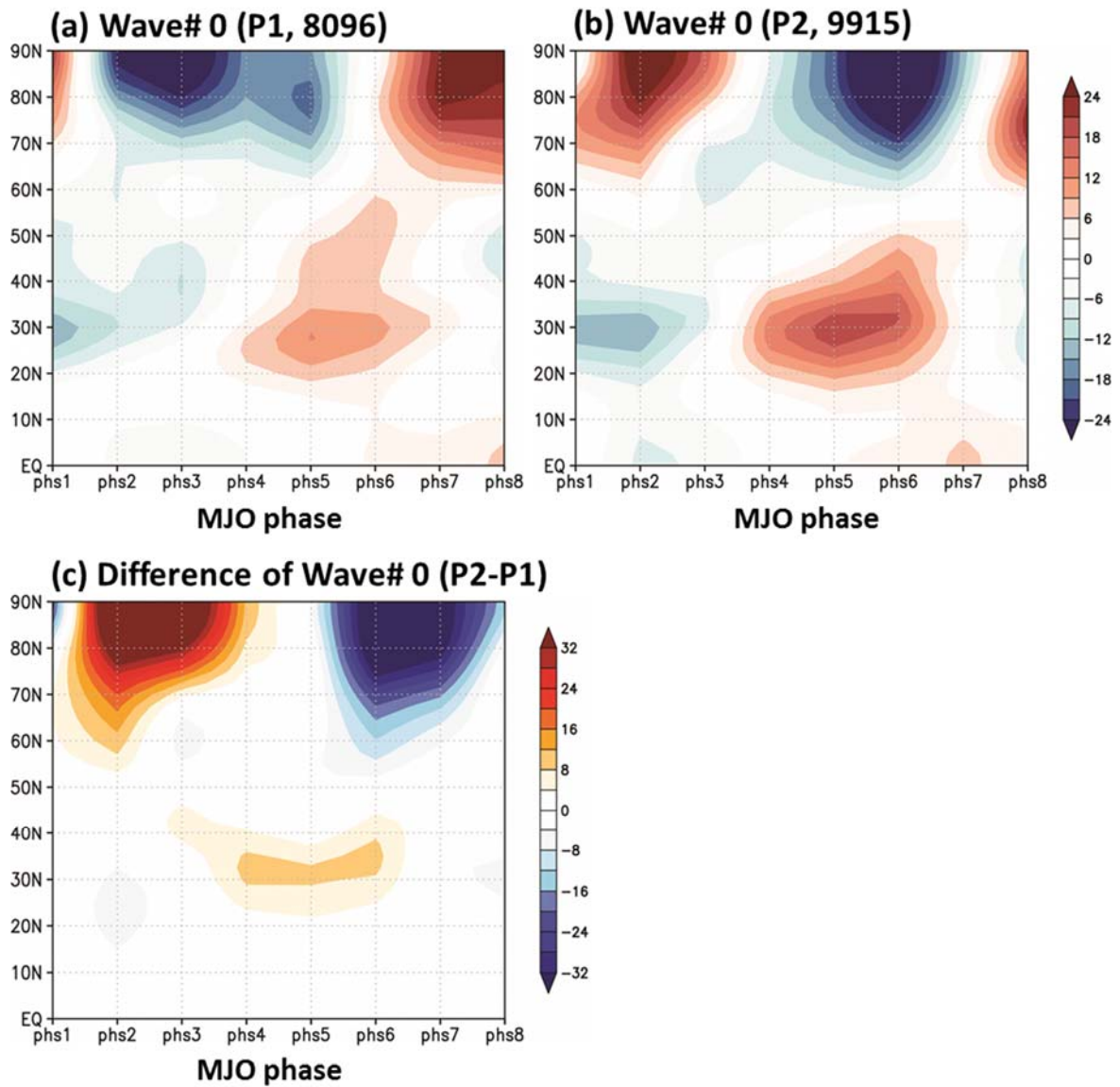


Figure 2.4.11 Zonal mean of the 20-100 days filtered GPH200 anomaly at 200hPa over the whole longitude with zonal wavenumber 0.

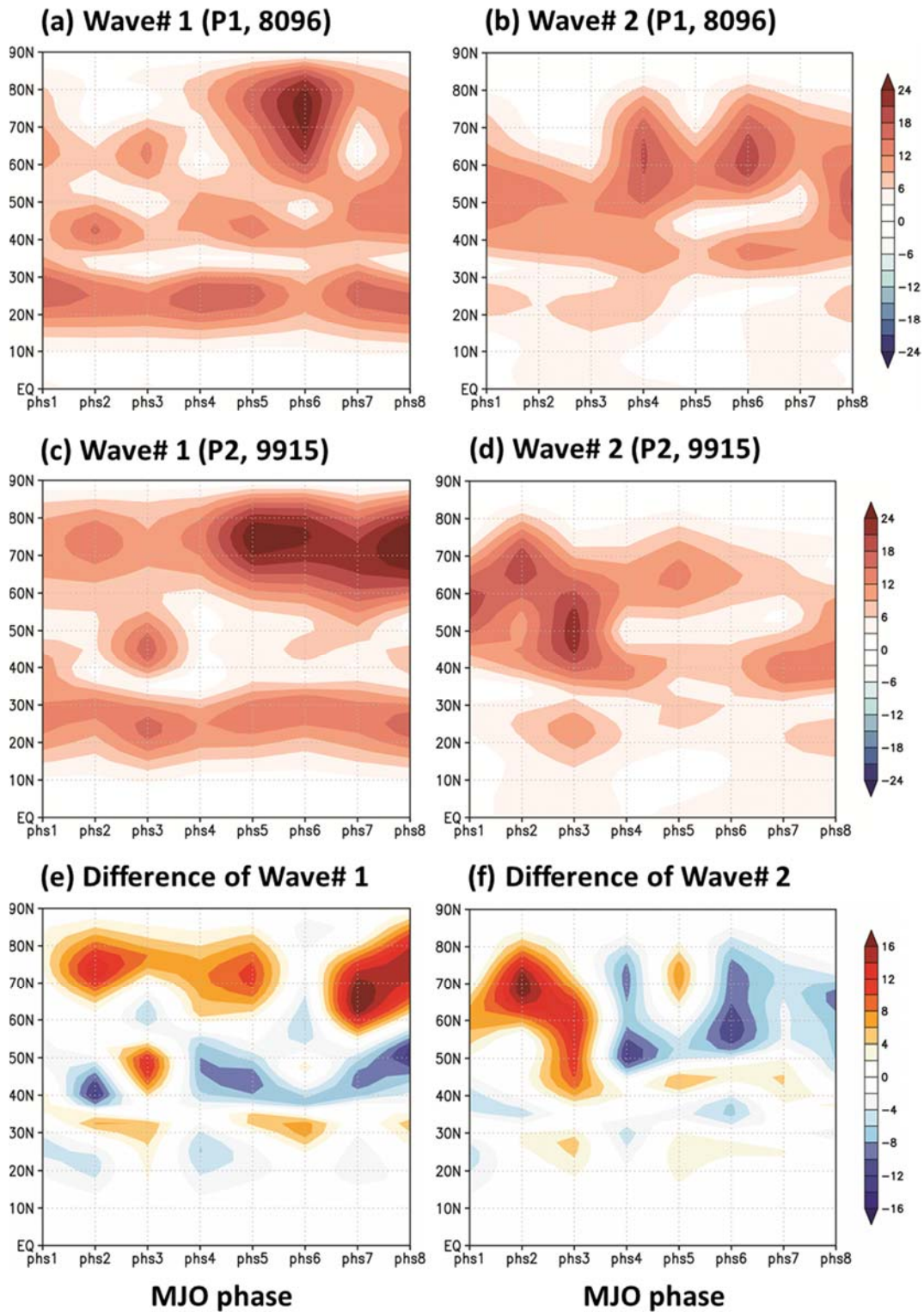


Figure 2.4.12 Zonal mean of intensity of the 20-100 days filtered GPH200 anomaly at 200hPa with zonal wavenumber 1 and 2. The intensity is defined as square root of square of the value averaged over whole longitude ($\sqrt{\text{average}(gph * gph, lon = 0, lon = 360)}$).

2.5. Summary

MJO teleconnection pattern is affected by tropical MJO activity and background states. Thus, it is important to investigate that change of climate modulates background states over the extratropics and MJO activity over the tropics, and to understand how these changes influence on MJO teleconnection pattern to predict MJO teleconnection pattern caused by changes of background states and MJO activities according to climate change such as decadal variation or global warming. Based on this importance, this study examines decadal changes of wintertime MJO teleconnection patterns and factors, such as MJO activity and background states that modulate the MJO teleconnection pattern using observation data.

In boreal winter for the recent period (P2, 1999-2015), the 20-100 days filtered OLR variance is strengthened over the Maritime Continent and the northern Indian Ocean and is weakened over the southern Indian Ocean, the western Pacific and the South Pacific Convergence Zone (SPCZ). However, this is inconsistent with the result, in which the frequency of the recent MJO occurrence has changed little at most MJO phases except for MJO phase 6. In contrast, the frequency result, the results of MJO amplitude at each MJO phase based on OMI tend to account for the decadal change of tropical diabatic heating.

It is thought that the change of MJO activity is associated with the decadal change of background states in tropics. Because the characteristics of background states over the tropics in the recent period resembles the La Nina year in comparison to the past period, that is, there is upwelling motion over the Maritime Continent, and at the same time, specific humidity at low-level and relative humidity (RH) also increase over the same region. On the other hand, downwelling motion exists over the central and eastern Pacific, and the specific humidity and RH decrease. These changes in intensity, location, and occurrence frequency of the filtered OLR anomaly will alter the MJO teleconnection pattern.

The location of MJO teleconnection patterns can be determined by seasonal mean upper-level zonal wind acted as a waveguide. Based on this, decadal change of zonal wind at 200 hPa between two periods, P2 and P1, is investigated, and the obvious change of the jet stream is found, especially over the eastern Pacific. Over this region, stationary Rossby wavenumber (K_s) is expanded east and northward in the recent period than that in the past period. This change modifies the location and intensity of the teleconnection patterns based on the analysis of zonal wavenumber.

Chapter 3

3. Contribution of tropical heating and mid-latitude mean state to decadal change of MJO teleconnection pattern

3.1. Background

In the previous chapter, we looked at the decadal change in the MJO teleconnection pattern and two factors, tropical diabatic heating and background states at the mid-latitude, which influence on the MJO teleconnection pattern between the two periods. In addition, how these two factors affect the MJO teleconnection patterns is identified and outlined based on the previous studies. Based on these information and knowledge, in this chapter, we will examine which of the two factors has a more significant effect on the decadal change of the MJO teleconnection pattern by conducting GFDL model experiments.

3.2. Model experiment

3.2.1. Contribution

The spectral dry dynamical core of an atmospheric general circulation model of the Geophysical Fluid Dynamics Laboratory (GFDL) is used to investigate the contribution of the two factors to the decadal change of the wintertime MJO teleconnection pattern. This model is a primitive equation model and has spatial resolution T42L20 (approximately 2.8° x approximately 2.77°). The tropical relaxation simulations are conducted by nudging vertical profiles of prognostic variables as the reference state, which is a similar method as Hoskins et al. (2012). The tropical relaxation over a specified nudging domain generates anomalous atmospheric teleconnection out of nudging domain against a constant forcing maintaining climatology. A differential damping in the three lowest levels (0.975, 0.925 and 0.875 sigmas) for wind with a damping time scale of 1.5, 2.5, and 4 days and 0.375, 0.625 and 1 days over ocean and land, respectively. The Newtonian cooling and vertical diffusion with a mixing coefficient of $5 \text{ m}^2 \text{ s}^{-1}$ are included in the model.

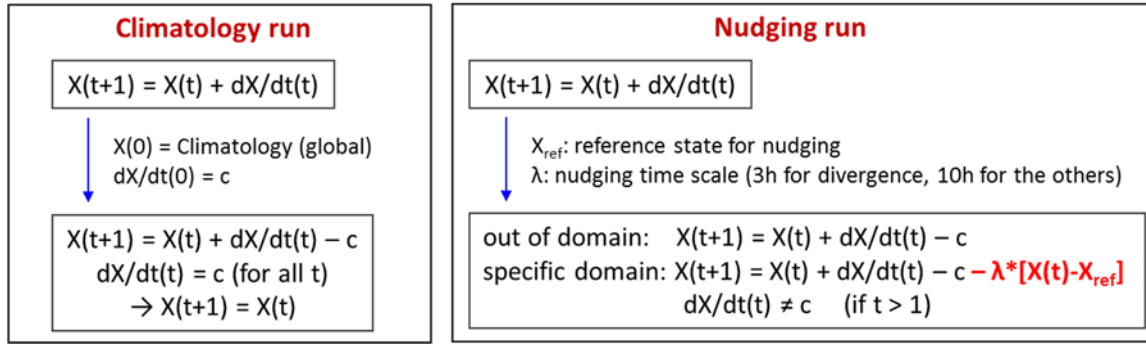


Figure 3.2.1 Configuration of GFDL model.

The variables obtained from ERA-interim reanalysis data is used for the data as an input data, which input variables used for the model experiment are surface pressure (Ps), vertical zonal wind (U), meridional wind (V), and temperature (T). The period and the season are the same as the data and method in Chapter 2, that is, the period 1 (P1, the past period) and period 2 (P2, the recent period) are 1980-1996 and 1999-2015, respectively, and the boreal winter is defined as November to March as an extended winter. The background fields are obtained from the climatological seasonal-mean for each period. The forcing data is the 20-100 days filtered OLR anomalies at each MJO phase for each period (Not eastward-moving) that is calculated using composite method, and the forcing domain is confined over the only tropical region (longitude 0-360 and latitude 30S-20N).

The climatology and the nudging runs from the model experiment maintain the climatological fields of variables over the out of and specific domains, respectively, by subtracting constant forcing at each time step, which acts as a resting basic state with additional forcing as shown in figure 3.2.1. At each time step of 1,200 seconds, the model prognostic variables (divergence, vorticity, temperature, and surface pressure) are relaxed towards reference states. The nudging time scale of divergence is 3 hours, and the other variables are 10 hours. Figure 3.2.1 shows a brief explanation for the GFDL model configuration.

3.2.2. Verification of model experiment

To investigate how the decadal changes in the tropical forcing and the background states contribute to the decadal change of the MJO teleconnection pattern, the GFDL model experiments are established as delineated in table 3.2.1. In experiment 1 (hereafter, Exp1), the background states and the tropical forcing for P1 are used, on the other hand, in experiment 2 (hereafter, Exp2), the background states and

the tropical forcing for P2 are applied. These simulations from these experiments are used for the reproducibility of the GFDL model. Experiment 3 (hereafter, Exp3) adopts the background states for P1 and the tropical forcing for P2, but experiment 4 (hereafter, Exp4) uses the background states for P2 and the tropical forcing for P1 conversely. For a fair comparison with the observed results, we use geopotential height at 224.536hPa from the model simulation, which is analogous to the vertical level (200hPa) from the observation. In addition, since the output data are produced by applying variables with the intraseasonal variability to the climatological fields, we can assume that the output data have the intraseasonal variability. Thus, hereafter, this is referred to as the GPH200 anomaly like the results from the observation.

Figure 3.2.2 displays the saturation time of the upper-level circulation anomaly after the tropical forcing with the intraseasonal variability applying to the tropics in the model experiments. The time unit is day. The results over East Asia (EA) and North America (NA) where the MJO teleconnection pattern has developed are compared using the intensity of the GPH200 anomaly. Over EA, the intensity of the teleconnection pattern is saturated at approximately five days and approximately ten days over NA at most MJO phases. Therefore, the MJO teleconnection patterns are compared at lag ten days when the teleconnection patterns are saturated to avoid the change of the spatial distribution of the teleconnection patterns as they develop.

Table 3.2.1 Information on model experiments

	Exp1	Exp2	Exp3	Exp4
Background	1980-1996 (P1)	1999-2015 (P2)	1980-1996 (P1)	1999-2015 (P2)
Tropical Forcing	MJO phase (P1)	MJO phase (P2)	MJO phase (P2)	MJO phase (P1)
Abbreviation	b1f1	b2f2	b1f2	b2f1

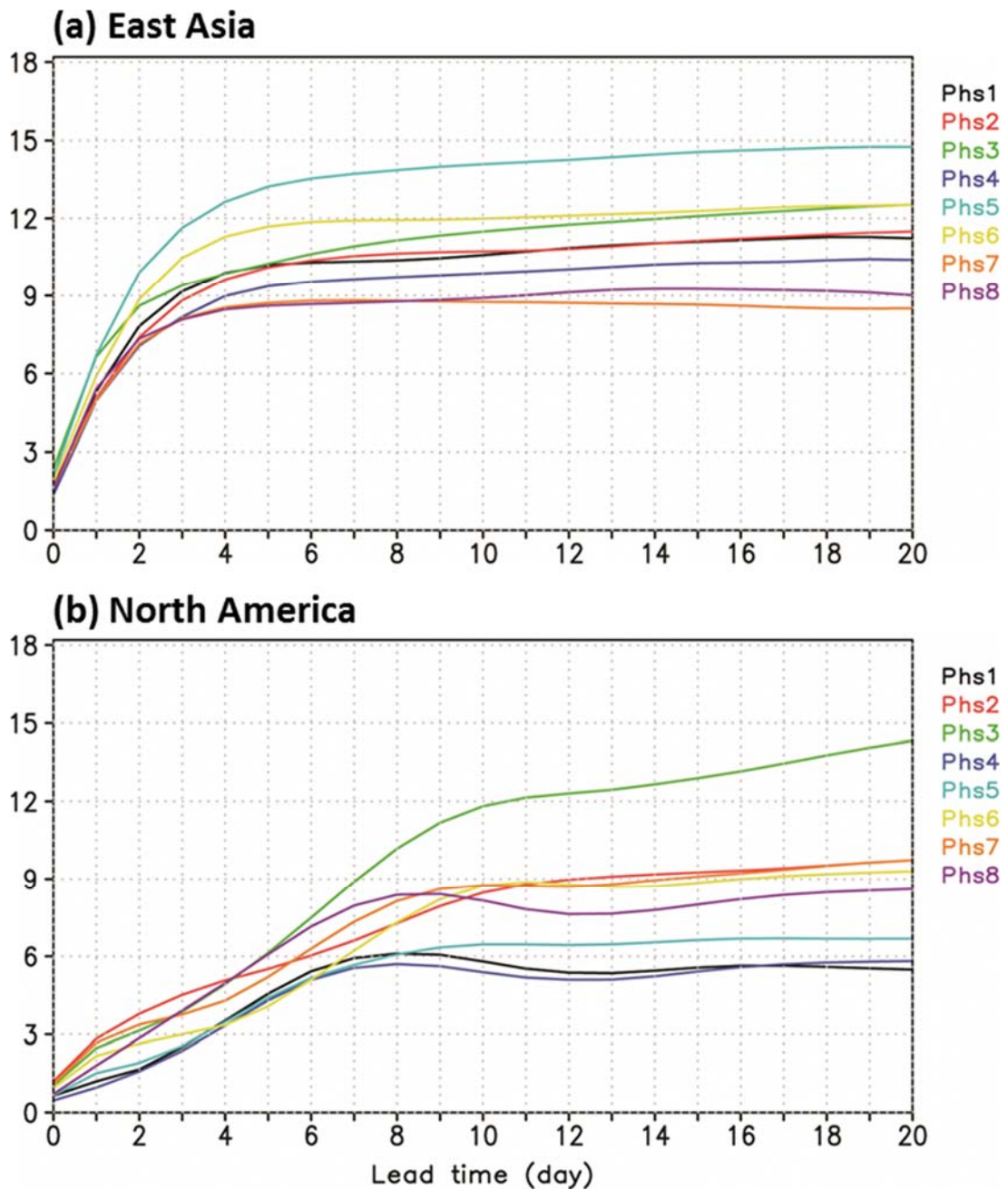


Figure 3.2.2 Intensity of the GPH200 anomaly at the upper-level averaged over (a) East Asia (EA, longitude 90-160E and latitude 20-60N) and (b) North America (NA, longitude 160E-30W and latitude 20-80N) from Exp2. The intensity is defined as $(\sqrt{(gph\ anomaly * gph\ anomaly)})$.

Figure 3.2.3 and 3.2.4 represent that the MJO teleconnection patterns from the observation and the model simulations are compared by averaging two MJO phases, such as the phase 2-3 and 6-7, when the strong MJO cases appear. The composite method is used to obtain the observed teleconnection patterns, and these teleconnection patterns are similar to each other, the observation and the model simulation. The spatial distributions of the MJO teleconnection patterns at MJO phase 2-3 and phase 6-7 from Exp1 (Exp2) and the observation for P1 (P2) are analogous, especially over the subtropical region and the upstream region of the teleconnection pattern, although there is the obvious difference over the downstream region, such as the European Continent. Thus, the model tends to reproduce reasonably the decadal change of the teleconnection pattern over the upstream regions, the North Pacific, and North America.

The spatial correlation coefficients of the MJO teleconnection patterns are calculated to confirm the similarity between the observation and the model simulation quantitatively. To validate the reproducibility of the MJO teleconnection pattern, the teleconnection patterns from the observation and the simulation are averaged over the MJO phase 2-3, 4-5, 6-7, and 8-1 like figure 3.2.3 and 3.2.4. Figure 3.2.5 displays that most MJO phases from the Exp1 and Exp2 have a spatial correlation coefficient over 0.5 except for the MJO phases 2-3 and 8-1 from Exp1 that show the correlation coefficient approximately 0.48. Thus, it is considered that the contribution of the two factors to the decadal change of the MJO teleconnection patterns with the intraseasonal variability can be identified using this GFDL model and these model experiments.

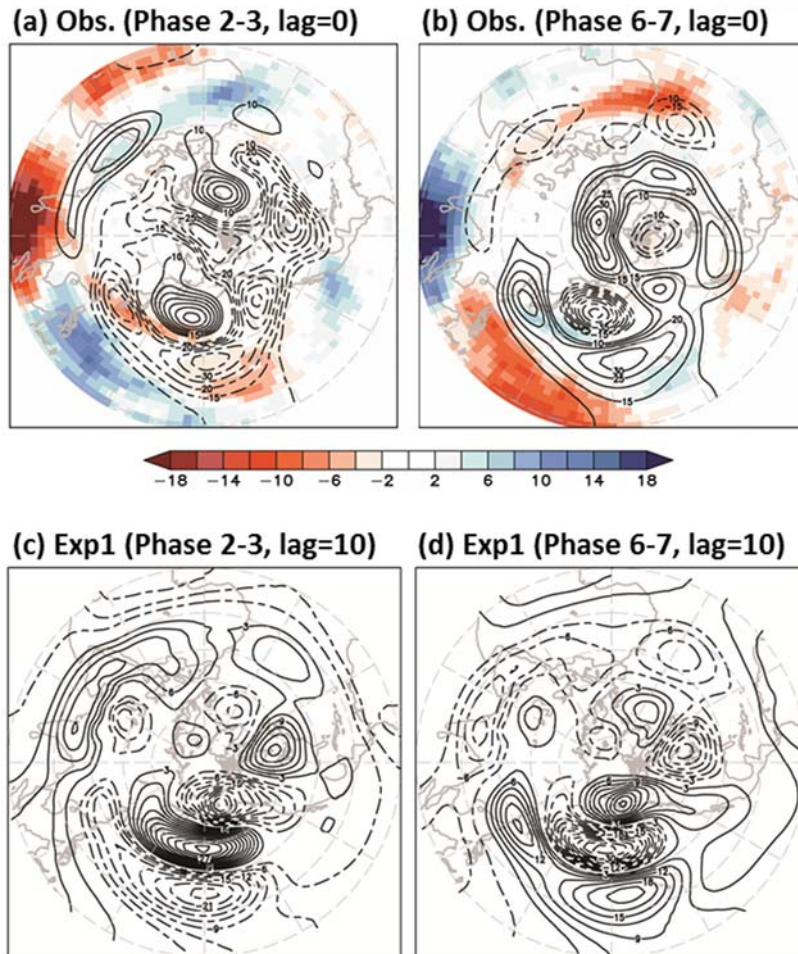


Figure 3.2.3 MJO phase-mean MJO teleconnection patterns represented by the GPH anomaly at the upper-level from the observation (top) and the simulation from Exp1 (bottom). Results from the observation are the 20-100 days filtered GPH anomaly at 200hPa at lag 0 days, and from the model, simulation is GPH anomaly at 224.536hPa at lag ten days. The results are averaged over MJO phases 2 and 3, and 6 and 7.

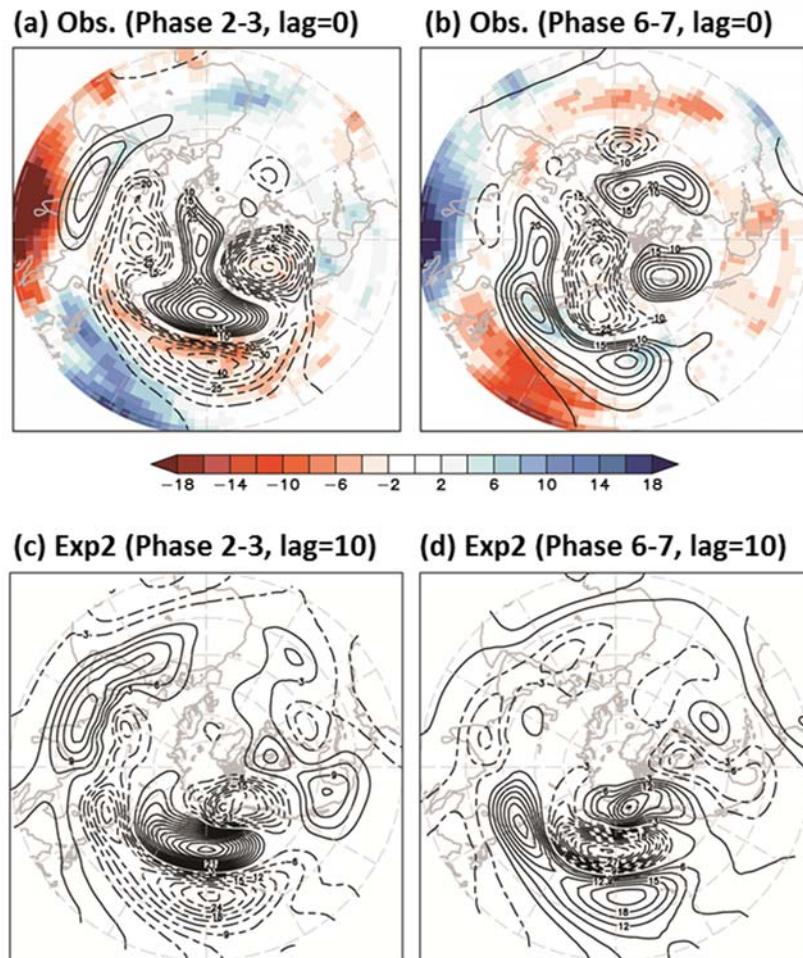


Figure 3.2.4 Same as Figure 3.2.3 except for Exp2.

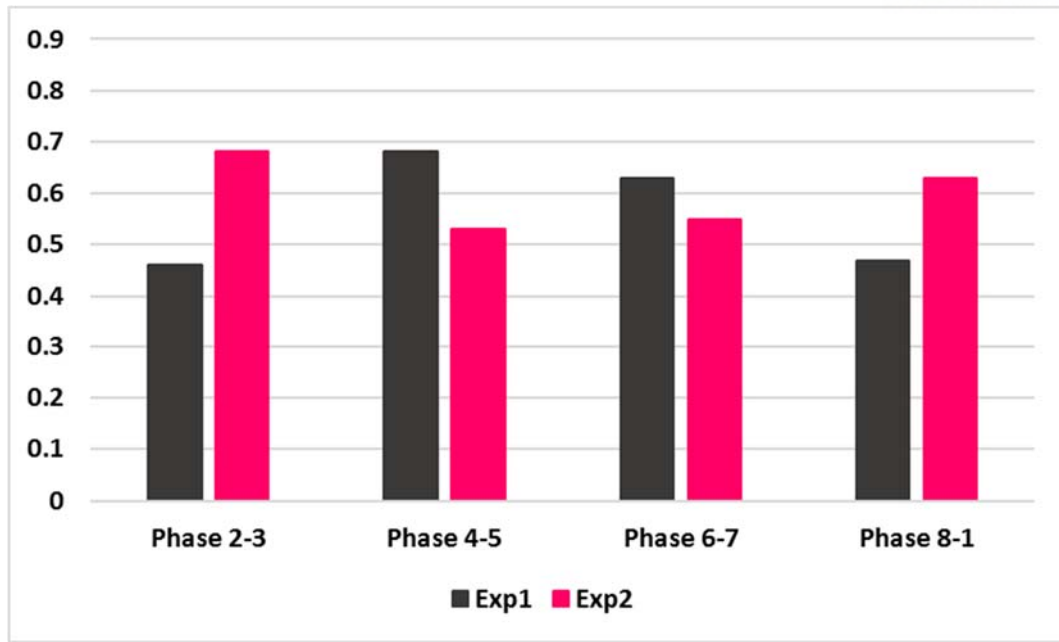


Figure 3.2.5 Spatial correlation coefficients between the model experiment, Exp1 and Exp2, and the observation. The coefficients are averaged over the northern hemisphere (longitude 0-360 and latitude 10-90N), and over the two phases, such as 2-3, 4-5, 6-7, and 8-1.

3.3. Contribution of two factors to the decadal change of MJO teleconnection

3.3.1. Role of tropical heating and mid-latitude mean state in the decadal change of MJO teleconnection pattern

Based on the GFDL model experiments shown in table 3.2.1, roles of the tropical diabatic heating and the mid-latitude background states in the decadal change of the MJO teleconnection pattern are identified. First, we develop a hypothesis that the decadal change of the zonal wind at the upper level as a background state will modify the location and intensity of the MJO teleconnection patterns more dominantly in comparison to the decadal change of the tropical forcing, particularly over the upstream region.

Figure 3.3.1 and 3.3.2 describe the simulated GPH200 anomalies at the upper level averaged over the two MJO phases, 2-3 and 6-7. When Exp 1-4 are compared, the all experiments describe similar MJO teleconnection patterns. However, the difference maps display the contribution of the two factors clearly. For instance, the different background states but the same tropical forcing obtained from the recent period are adopted from Exp2 and Exp3 shown in figures 3.3.1-d and 3.3.2-d, then the MJO teleconnection patterns from these experiments are reproduced similarly to each other. And, the results in figures 3.3.1-d and 3.3.2-d show that the teleconnection cells over the Pacific and North America are strengthened over the jet exit region in the mid-latitude. This change is consistent with the increase of kinetic energy over the jet exit region based on the Rossby wave dynamics explained in Chapter 2. However, contrary to this, when the same background states taken from the past period, but the different tropical forcing is used, the MJO teleconnection patterns are modified more strongly than those from the experiments that the different background states are adopted from Exp3 and Exp 1 shown in figures 3.3.1-e and 3.3.2-e. Especially, the teleconnection patterns are changed dominantly over the Pacific, North America and the northern Atlantic. This difference between the two experiments is seen in stronger and wider regions than figures 3.3.1-d and 3.3.2-d. Interestingly, this difference is analogous to the different patterns from the observation (figure 3.3.1-f and 3.3.2-f), and the regions where the significant differences occur are resembled based on the difference maps from the model simulations and the observation although the model simulations have difficulty in representing the MJO teleconnection patterns over the Arctic. These features can be seen at other MJO phases.

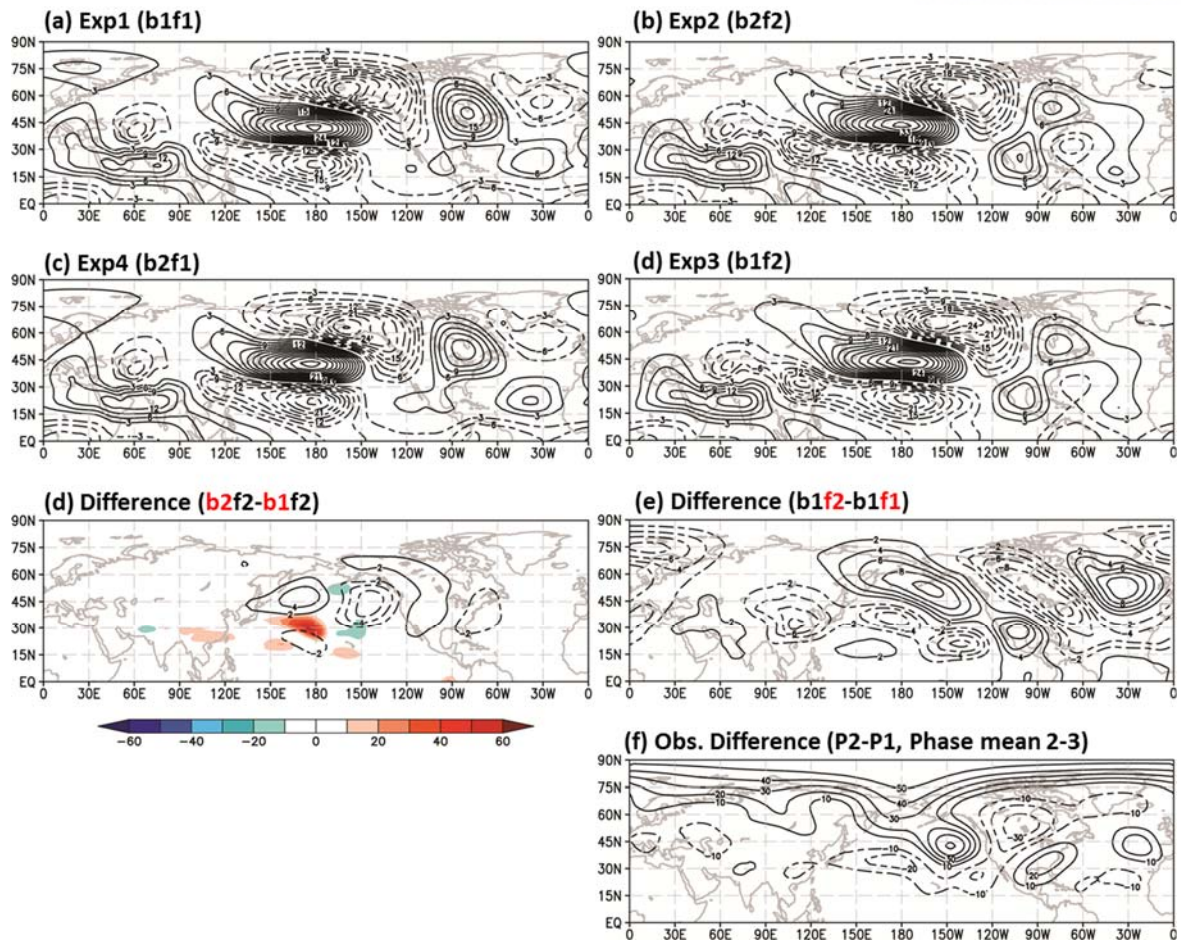


Figure 3.3.1 GPH200 anomalies at MJO phases 2 and 3 from the Exp1-4 (a-d) and its difference maps between Exp2 and Exp3 (d) and Exp3 and Exp1 (e). (f) is the difference map of the observed GPH200 anomaly between P2 and P1.

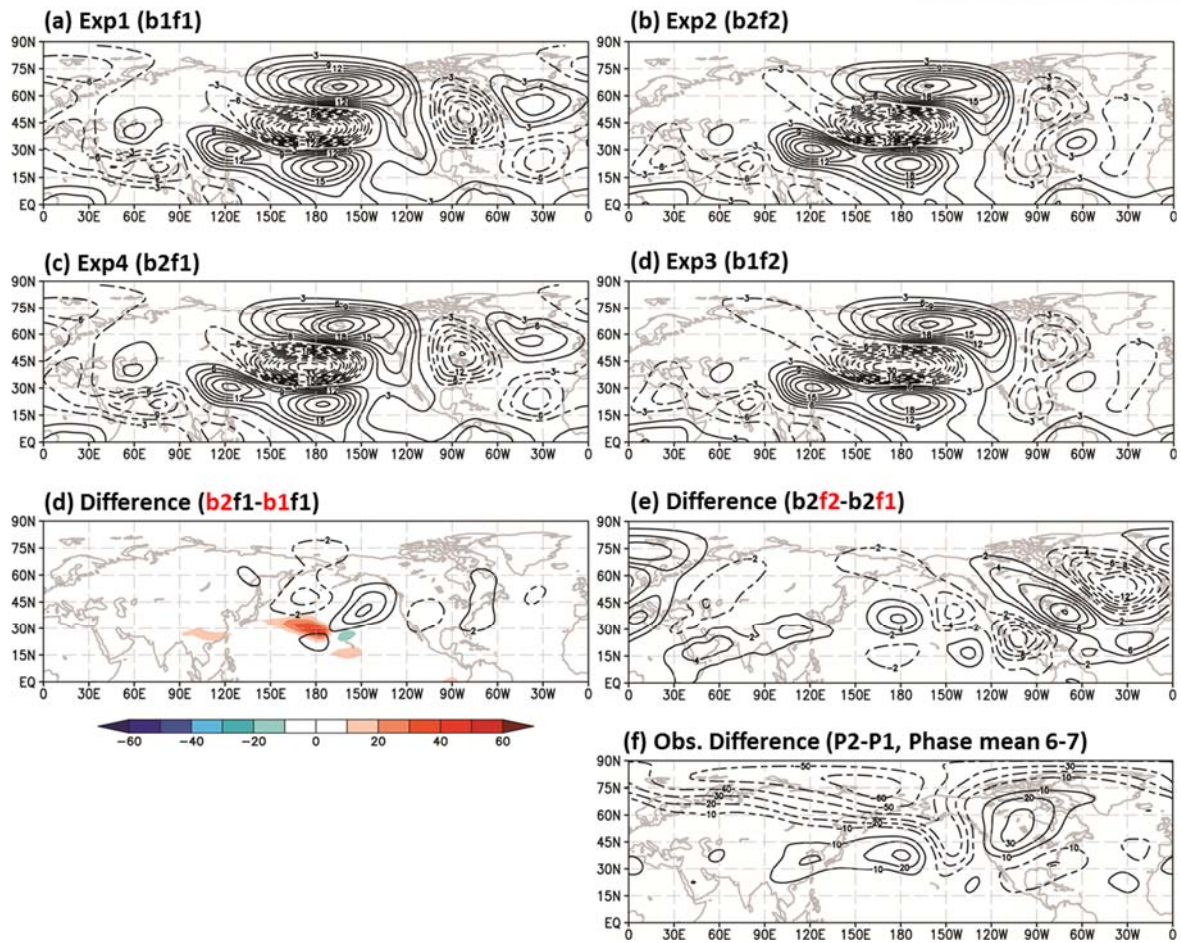


Figure 3.3.2 Same as Figure 3.3.1 except for MJO phases 6 and 7. Difference maps between Exp4 and Exp1 (d) and Exp2 and Exp4 (e).

The spatial correlation coefficients are calculated and compared between the model experiments to quantify the similarity or the dissimilarity. Figure 3.3.3 displays that there are higher correlation coefficients when the same tropical forcing is adopted than the same background states are adopted in consistent with figure 3.3.1 and 3.3.2. Therefore, these results suggest that the decadal change of the MJO teleconnection pattern between the two periods, P1 (1980-1996) and P2 (1999-2015) is caused by the decadal change in the tropical diabatic heating associated the MJO rather than the decadal change in the seasonal-mean zonal wind in the mid-latitude as background states.

We should be also be careful when accepting these conclusions. The first reason is that the MJO is originally an eastward-propagating phenomenon, but in these experiments, this eastward-propagating feature is ignored because the tropical diabatic heating, that is the MJO-related OLR anomaly, is obtained by using the composite method. Thus, we can not expect an influence of the eastward propagation. The second reason is a limitation of the GFDL model. The simple and primitive equation model like the GFDL model used in this study has many limitations, and one of them is that the model tends to have difficulty in describing the teleconnection pattern over the Arctic. For example, in Chapter 2, there are the obvious decadal changes in the observed teleconnection pattern with zonal wavenumber 0 and 1 over the high latitudes and the Arctic, but these results from the model simulations do not show the teleconnection patterns realistically, even rarely, over the Arctic and the high latitudes. Given these limitations, it is considered that the interpretation of the decadal changes over the high latitudes and the Arctic should be made carefully.

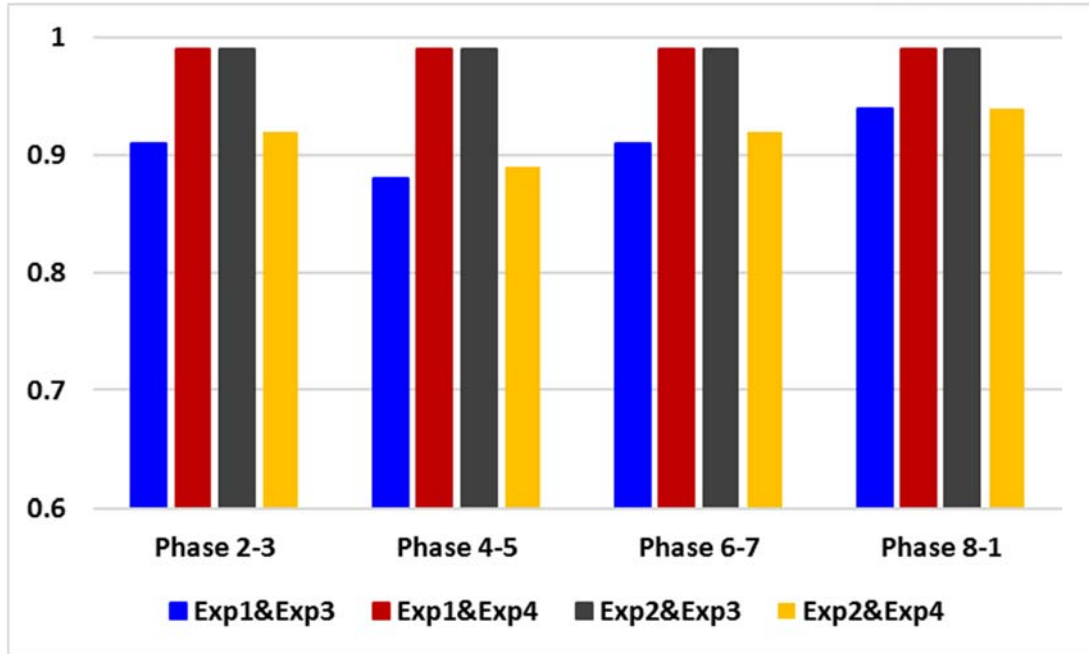


Figure 3.3.3 Spatial correlation coefficients between the model experiments. The coefficients are averaged over the northern hemisphere (longitude 0-360 and latitude 10-90N) and over the two phases, such as 2-3, 4-5, 6-7, and 8-1.

3.3.2. Effect of seasonal mean state on MJO teleconnection pattern

Based on the previous results and the limitations of this study, other scientific questions are emerged; did the decadal change in the wintertime zonal wind as the background state play a role properly in this model simulation? If we adopt the different seasonal-mean background states, do the spatial distribution of the MJO teleconnection patterns appear differently?

The model experiment conducts by using the wintertime tropical forcing, but the summertime background states to verify this, and the result from the simulation is compared with the result from the original Exp2. Figure 3.3.4-c and d describe that the MJO teleconnection patterns are not developed sufficiently over the Pacific and do not propagate eastward and northward into the northern Pacific and the North America when the summertime background states are adopted in compared to the patterns from the simulation with the wintertime background states at all MJO phases. That is, in the GFDL model, the background states play a proper role in formatting and propagating the Rossby wave, and it can be thought that the reason for the absence of the decadal change in the MJO teleconnection patterns used the wintertime background states is that the change in the background states is not significant enough to cause the decadal change of the MJO teleconnection pattern. Therefore, it is confirmed again that the decadal change in the MJO teleconnection patterns occurs due to the decadal change in the tropical convection not the background states over the tropics and in the mid-latitudes through these experiments

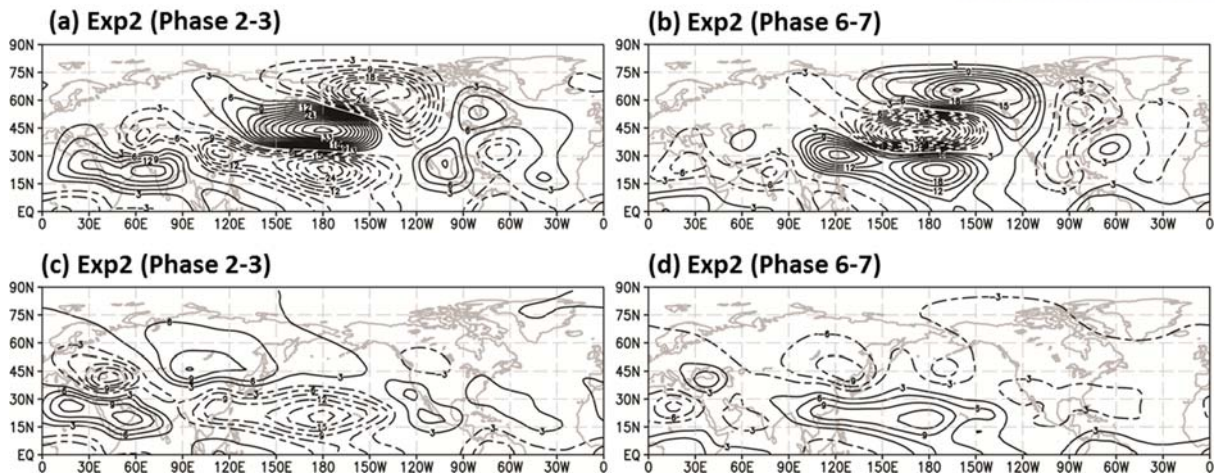


Figure 3.3.4 GPH200 anomalies at MJO phases 2-3 and 6-7 from Exp2. The simulated results from (a-b) and (c-d) are obtained by using the wintertime and the summertime background states, respectively. The same wintertime tropical forcing is applied to all experiments.

3.4. Relationship between decadal changes in tropical mean states and MJO teleconnection patterns

In the previous section, the results from various analysis explained that the decadal change in the tropical diabatic heating influences the decadal change in the MJO teleconnection patterns than that in the background states in the mid-latitude.

So, why did the MJO-related diabatic heating change take place over the tropics?

As explained earlier, in the recent period, the background states over the are changed into La Nina-like pattern, and moisture and SST increase over the Indian Ocean, Maritime Continent, and the western Pacific. In addition, the ascending motion of the vertical circulation in the background states strengthens over the eastern region of Maritime Continent, and then the convective anomaly becomes stronger over the same region in the recent period than in the past period. It is thought that these background changes including the intensification of the vertical circulation lead to the enhancement of the MJO teleconnection pattern and its teleconnectivity over the upstream regions, such as the northern Pacific and the North America.

An influence of ENSO on the MJO teleconnection patterns during boreal winter is investigated in many previous studies, Moon et al. (2011) and Kim et al. (2017), and this implies that the MJO teleconnection patterns are changed according to El Nino and La Nina phases. Thus, in this section, the MJO teleconnection patterns according to ENSO phases are examined for the whole period (1980-2015). The El Nino, La Nina and neutral years are determined based on the NOAA Climate prediction center (hereafter, CPC). The El Nino and La Nina years are defined based on a threshold of $\pm 0.5^{\circ}\text{C}$ for the Oceanic Niño Index (ONI), which is calculated by conducting 3 month running mean of SST anomalies in the Niño 3.4 region (5S-5N, 120-170W). The El Nino years are 1982, 1986, 1987, 1991, 1994, 1997, 2002, 2004, 2006, 2009, and 2014, the La Nina years are 1983, 1984, 1988, 1995, 1998, 1999, 2000, 2005, 2007, 2008, 2010, and 2011, and the neutral years are 1980, 1981, 1985, 1989, 1990, 1992, 1993, 1996, 2001, 2003, 2012, and 2013. The composite method is used for these results for each ENSO phase to compare fairly with the MJO teleconnection patterns for the two periods.

Figure 3.4.1 and 3.4.2 show the comparison of the MJO teleconnection patterns at MJO phase 3 and 7 for P1, P2, El Nino and La Nina years. The teleconnection patterns at MJO phase 3 shown in figure 3.4.1 represent the close relationship between P1 and El Nino years or P2 and La Nina years, especially, in cases of the location and the intensity of the teleconnection patterns over the upstream region. However, at MJO phase 7, the similarity of the teleconnection patterns in P1 and El Nino years or P2

and La Nina years is almost absent, and this indicates that its dependence on ENSO phases is different according to the MJO phase. Furthermore, these results are not dependent on the number of El Nino or La Nina years since the MJO teleconnection patterns for El Nino and La Nina year including 1996-1998 are not changed significantly even though the 1997 and 1998 are strong El Nino and La Nina years, respectively. Particularly, these results in this study are also compared with the previous studies, such as Moon et al., (2011) and Kim et al. (2017). The results from the previous studies and the teleconnection patterns from this study show the similar spatial distribution and the intensity of the MJO teleconnection pattern. In other words, the feature that the teleconnection cells are more enhanced over North America during the La Nina phase than the El Nin phase is also observed in the teleconnection in P2. Figure 3.4.3 and 3.4.4 are supplementary figures and represent the MJO teleconnection patterns at all MJO phases for El Nino and La Nina years, but the results from figure 3.4.4 are composited for El Nino and La Nina years including 1996-1998.

To quantify the relationship of the MJO teleconnection patterns for P1 and P2, and El Nino and La Nina years, the spatial correlation coefficients are calculated at all MJO phases between P1 and El Nino years, P1 and La Nina years, P2 and El Nino years, and P2 and La Nina years. As described earlier, the MJO phase-averaged coefficients from MJO phase 1 to 8 for P1 (P2) and El Nino years and P1 (P2) and La Nina years are 0.62 (0.54) and 0.67 (0.74), respectively when 1996-1998 are excluded. Even if 1996-1998 are included, the spatial correlation coefficients are 0.63 (0.66), and 0.55 (0.74) for P1 (P2) and El Nino years and P1 (P2) and La Nina years, and not much different from the values excluded the two years (1996-1998). The similarity between the MJO teleconnection patterns for P2 and La Nina years is more definite than those for P1 and El Nino years although this relationship is found only at the MJO phase 1-5 except for the phase 2.

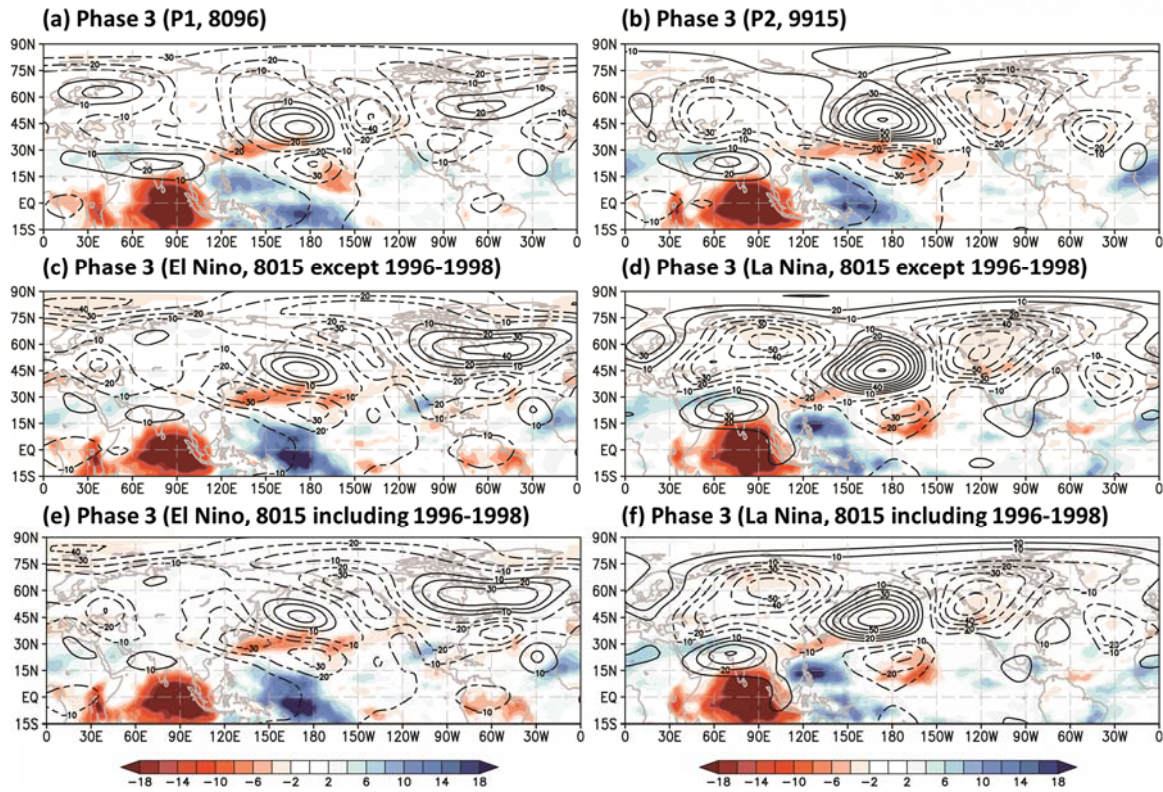


Figure 3.4.1 Composite maps of OLR (shading) and GPH200 (contour, 10m interval) anomalies filtered with 20-100 days at MJO phase 3 during boreal winter for (a) P1, (b) P2, (c) El Nino years and (d) La Nina years for the whole period except 1996-1998, and (e) El Nino years and (d) La Nina years for the whole period including 1996-1998. The units of OLR and geopotential height $W m^{-2}$ and m , respectively.

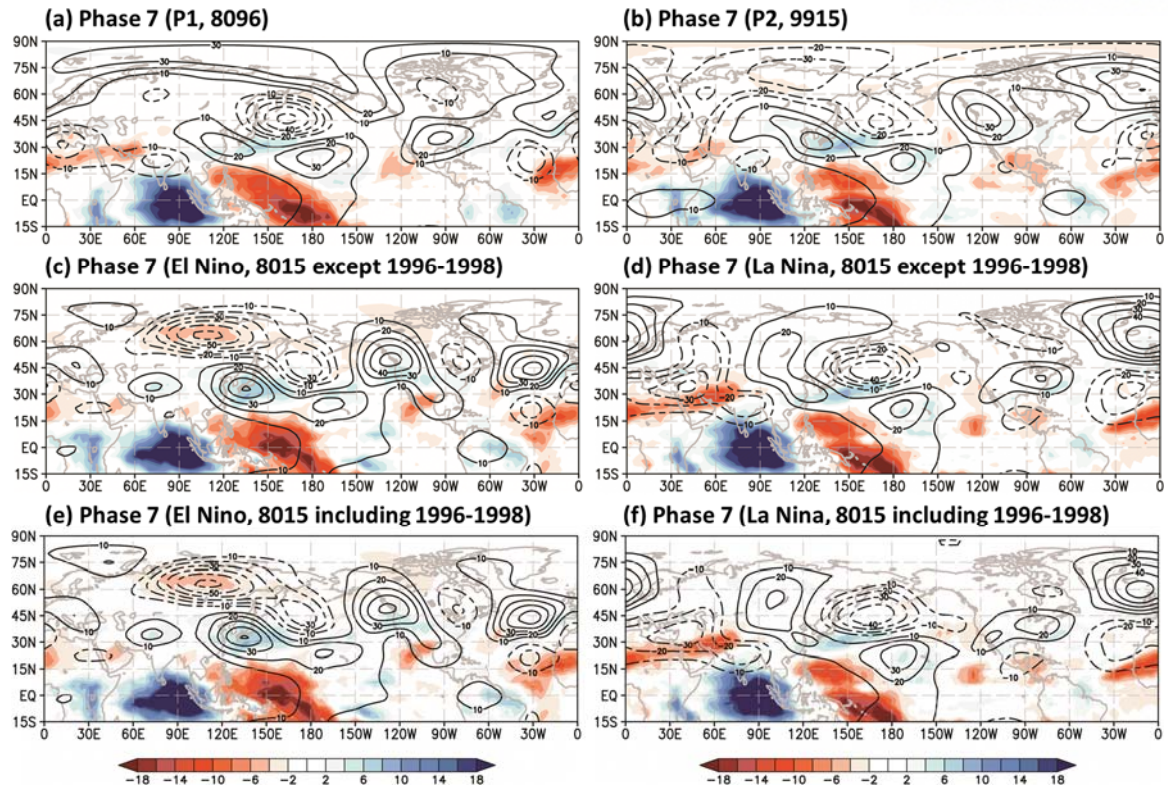


Figure 3.4.2 Same as Figure 3.4.1 except for MJO phase 7.

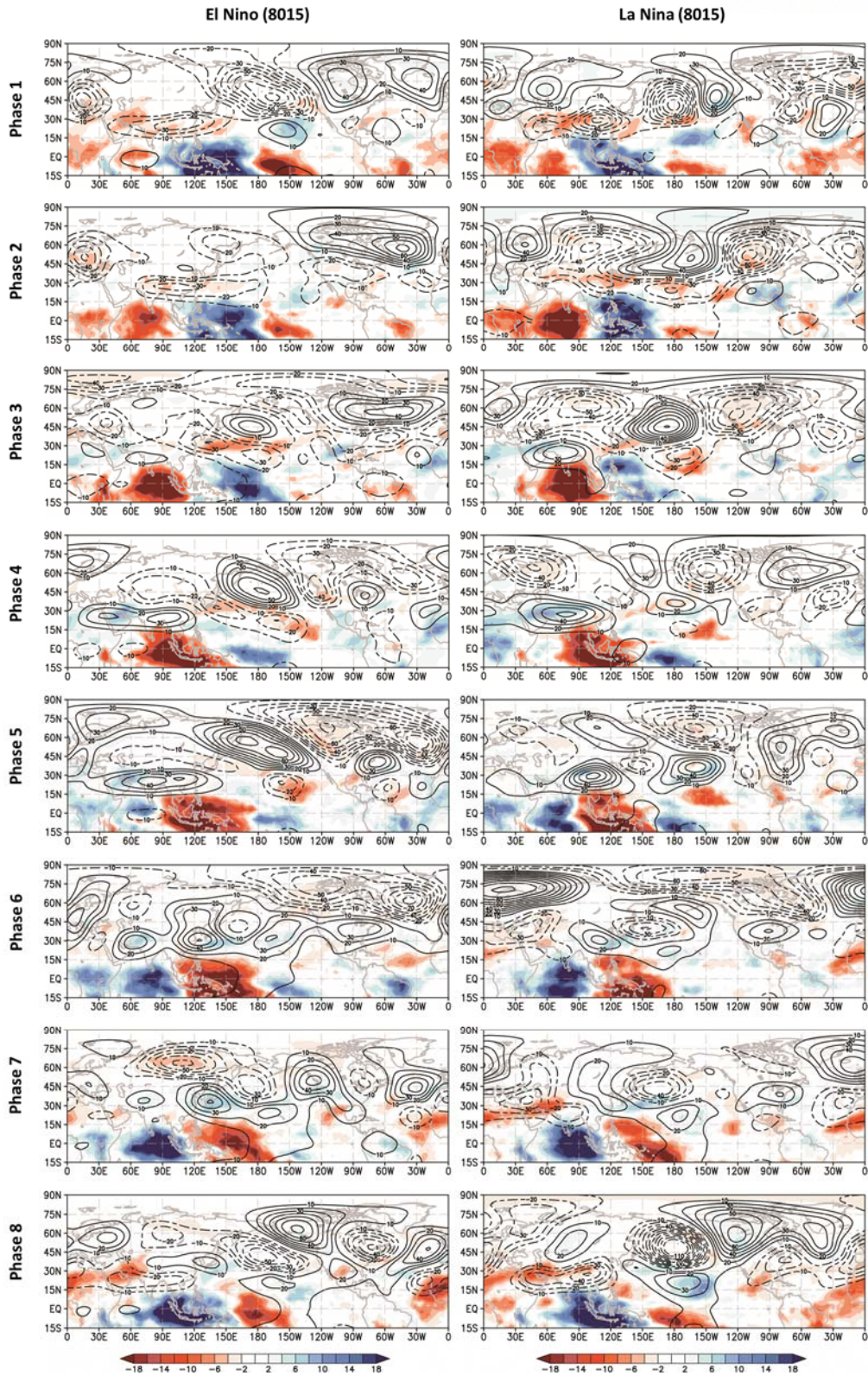


Figure 3.4.3 Composite maps of OLR (shading) and GPH200 (contour, 10m interval) anomalies filtered with 20-100 days at all MJO phases during boreal winter for (left column) El Nino years and (right column) La Nina years for the whole period except 1996-1998.

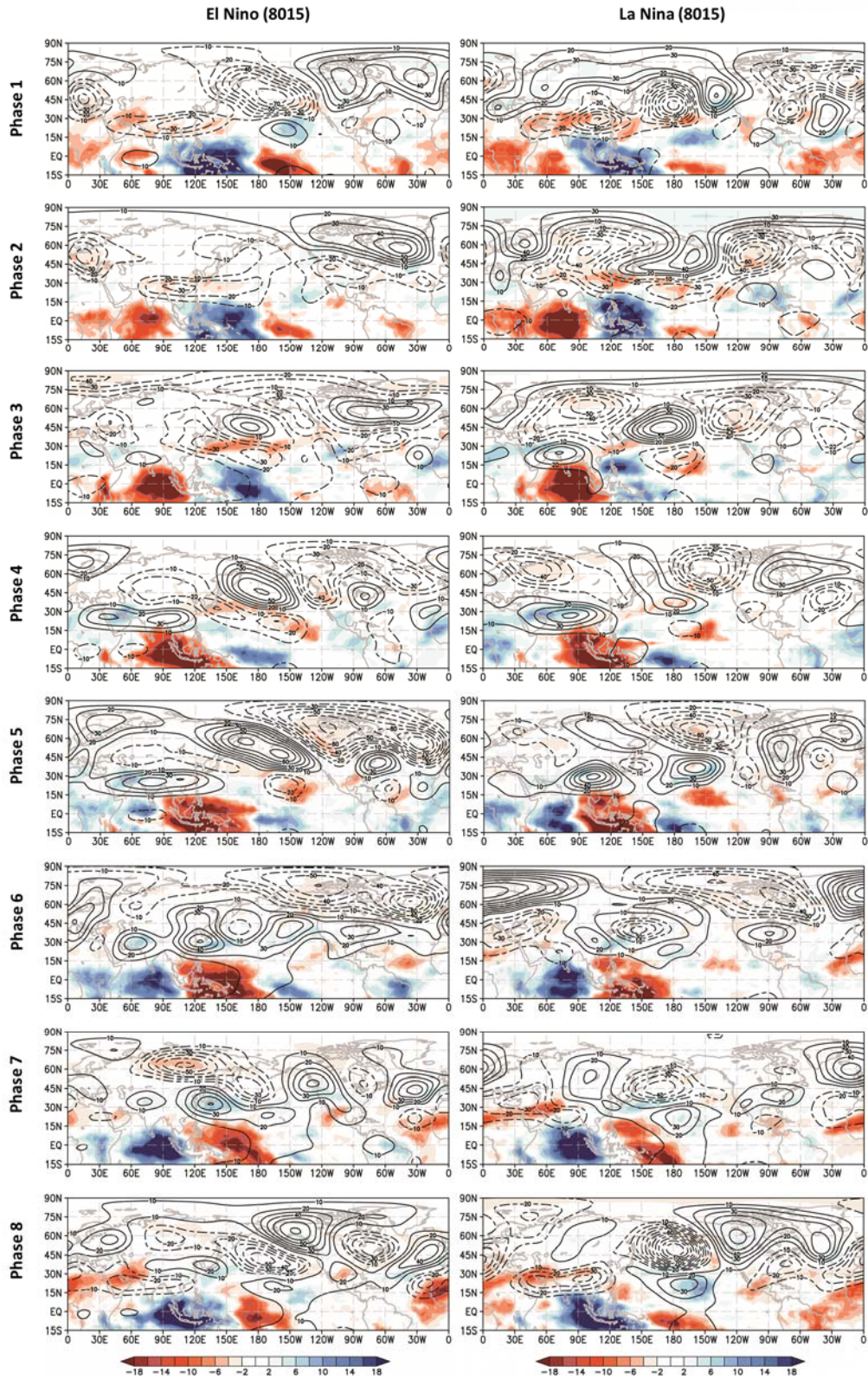


Figure 3.4.4 Same as Figure 3.4.3 except for the whole period including 1996-1998.

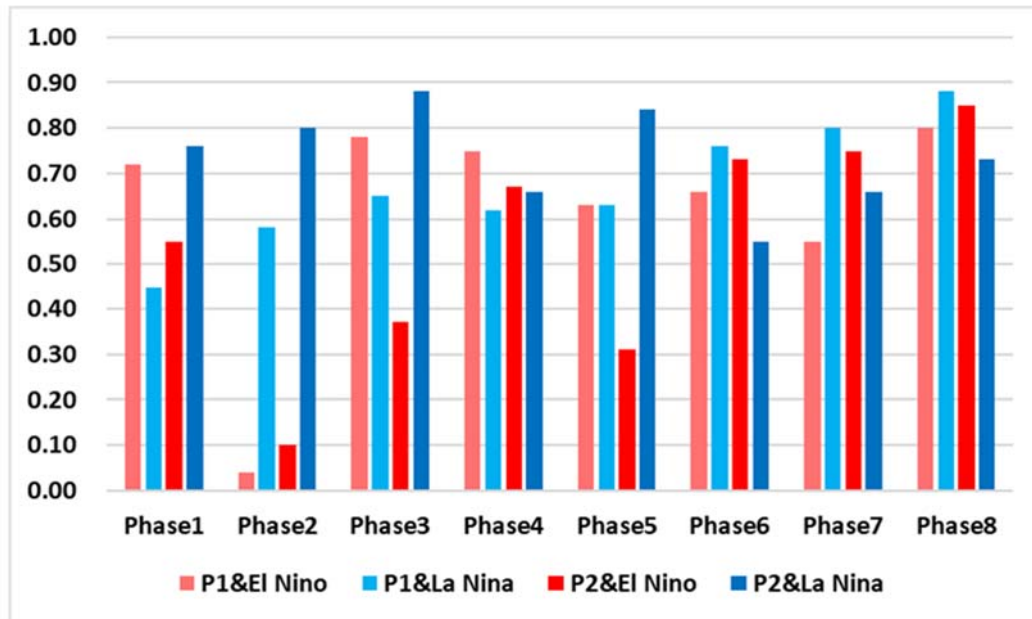
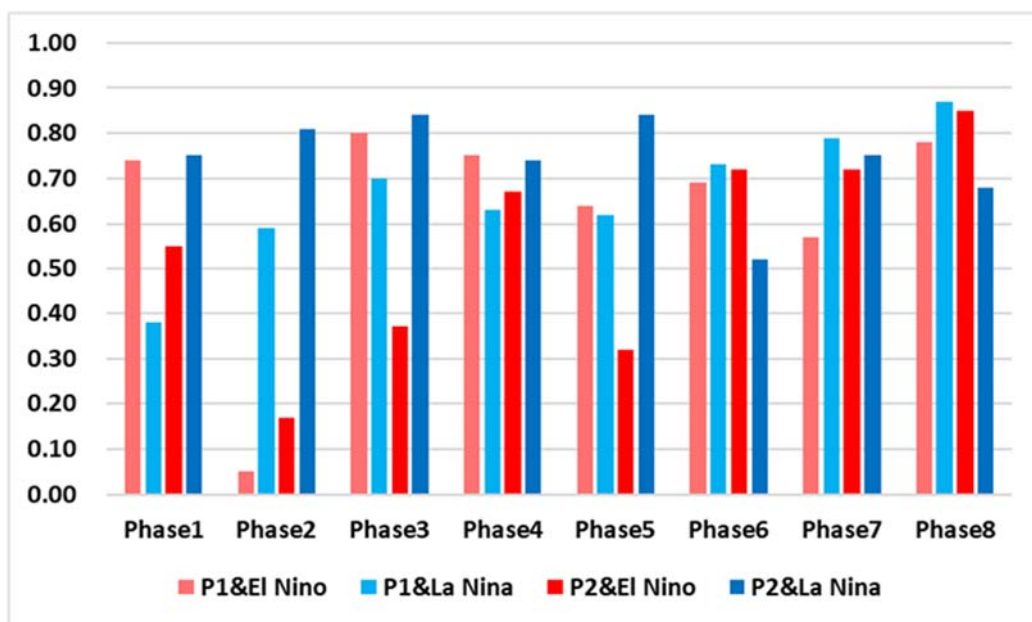
(a) Spatial correlation (8015 except 1996-1998)**(b) Spatial correlation (8015 including 1996-1998)**

Figure 3.4.5 Spatial correlation coefficients between the GPH200 anomalies obtained from the observation for P1, P2, El Nino and La Nina years. The correlation coefficients in (a) and (b) are obtained using El Nino and La Nina years for the whole period except and including 1996-1998, respectively. The coefficients are averaged over the northern hemisphere (longitude 0-360 and latitude 20-90N) at each MJO phase. Red- and blue-colored bars indicate the coefficients calculated with El Nino and La Nina years, respectively.

3.5. Summary

In this chapter, we looked at which of the changes in the two factors, the tropical forcing, and the background states, contributes more to the decadal change of the MJO teleconnection patterns. The decadal change in the background states, especially the zonal wind at the upper level as a background states, leads to strengthening the intensity of the MJO teleconnection pattern over the jet exit region but does not modify the pattern itself distinctly. On the other hand, the tropical heating modifies the MJO teleconnection patterns, particularly over the upstream region where is the North Pacific and North America, and these changes are similar to the different maps of the observation between P2 and P1. Thus, the results suggest that the decadal change of the MJO teleconnection pattern is mainly caused by the decadal change in the tropical diabatic heating rather than that in the zonal wind in the mid-latitude as background states.

Then, the decadal change in the MJO-related diabatic heating over the tropics is associated with the background states and is similar to La Nina-like pattern in the recent period. This leads to moisture and SST increase over the Indian Ocean, Maritime Continent, and the western Pacific. In addition, the ascending motion of the vertical circulation in the background states strengthens over the eastern region of Maritime Continent, and then the convective anomaly becomes stronger over this region in the recent period than in the past period. It is thought that these background changes including the intensification of the vertical circulation lead to the enhancement of the MJO teleconnection pattern and its teleconnectivity over the upstream regions, such as the northern Pacific and the North America.

Based on these results, the MJO teleconnection patterns are compared for P1, P2, El Nino and La Nina years, and this represents the close relationship between P1 and El Nino years or P2 and La Nina years, especially, in cases of the location and the intensity of the teleconnection patterns over the upstream region. However, its dependence on ENSO phases is different according to the MJO phase. Furthermore, these results are not dependent on the number of El Nino or La Nina years since the MJO teleconnection patterns for El Nino and La Nina year including 1996-1998 are not changed significantly even though the 1997 and 1998 are strong El Nino and La Nina years, respectively. The spatial correlation coefficients at all MJO phases between P1, P2, El Nino and La Nina years also represent the same results that the similarity between the MJO teleconnection patterns for P2 and La Nina years is more definite than those for P1 and El Nino years although this relationship is found only at the MJO phase 1-5.

Chapter 4

4. Conclusion

This study investigates the decadal change in the MJO teleconnection pattern during boreal winter over the Northern Hemisphere, and the influence of the decadal change in the background states in the mid-latitude and the tropical forcing on the MJO teleconnection pattern based on the analysis using the previous studies and the observational data. And, based on the results, the relationship and its dynamical mechanism are interpreted to predict the change of MJO teleconnection pattern according to climate change such as the decadal variation.

The MJO teleconnection patterns are affected by tropical MJO activity and the background states in the mid-latitude. Thus, it is important to understand how these changes influence on the MJO teleconnection patterns to represent the MJO teleconnection pattern caused by the decadal changes in the background states and the MJO activities over the tropics. In boreal winter for the recent period, the 20-100 days filtered OLR variance is strengthened over the Maritime Continent and the northern Indian Ocean and is weakened over the southern Indian Ocean and the western Pacific, and this is consistent with the results of MJO amplitude at each MJO phase based on OMI. This change of MJO activity is associated with the decadal change of background states in tropics. That is, there is upwelling motion over the Maritime Continent, and at the same time, specific humidity at low-level and relative humidity also increases over the same region. On the other hand, the downwelling motion exists over the central and eastern Pacific, and the specific humidity and RH decrease. These changes will alter the MJO teleconnection pattern. The location of the MJO teleconnection patterns can be determined by the seasonal mean upper-level zonal wind acted as a waveguide. Their obvious change of the upper-level zonal wind, that is jet stream, is found, especially over the eastern Pacific. Over this region, the stationary Rossby wavenumber is expanded east and northward in the recent period than that in the past period. This change modifies the location and intensity of the teleconnection patterns based on the analysis of zonal wavenumber.

Based on the model experiments using GFDL model, the decadal change of the background states, especially zonal wind at the upper level, leads to strengthening the intensity of the MJO teleconnection pattern over the jet exit region but does not modify the pattern itself. On the other hand, the tropical heating modifies the teleconnection patterns, particularly over the North Pacific and North America, and these changes are also found in the different maps of the observation between P2 and P1. Thus, the results indicate that the decadal change of the MJO teleconnection pattern is caused by the change of

tropical diabatic heating rather than the change of zonal wind in the mid-latitude as background states. These changes are associated with the background states are changed into La Nina-like pattern in the recent period. This leads to moisture and SST increase over the Indian Ocean, Maritime Continent, and the western Pacific. In addition, the ascending motion of the vertical circulation in the background states strengthens over the eastern region of Maritime Continent, and then the convective anomaly becomes stronger over this region in the recent period than in the past period. It is thought that these background changes including the intensification of the vertical circulation lead to the enhancement of the MJO teleconnection pattern and its teleconnectivity over the upstream regions. Furthermore, there is close relationship of the MJO teleconnection patterns between P1 and El Nino years or P2 and La Nina years, but, its dependence on ENSO phases is different according to the MJO phase, for example, the similarity between the MJO teleconnection patterns for P2 and La Nina years is more definite than those for P1 and El Nino years although this relationship is found only at the MJO phase 1-5.

References

- Ambrizzi, T., and Hoskins, B. J., 1997: Stationary Rossby-wave propagation in a baroclinic atmosphere. *Quarterly Journal of the Royal Meteorological Society*, 123, 919-928.
- Baxter, S., S. Weaver, J. Gottschalck, and Y. Xue, 2014: Pentad Evolution of Wintertime Impacts of the Madden-Julian Oscillation over the Contiguous United States. *J. Climate*, 27, 7356-7367.
- Bergman, J. W., H. H. Hendon, and K. M. Weickmann, 2001: Intraseasonal Air–Sea Interactions at the Onset of El Niño. *J. Climate*, 14, 1702–1719.
- Bond, N. A., Overland, J. E., Spillane, M., and Stabeno, P., 2003: Recent shifts in the state of the North Pacific. *Geophysical Research Letters*, 30.
- Branstator, 2002: Circumglobal Teleconnections, the Jet Stream Waveguide, and the North Atlantic Oscillation. *J. Climate*, 15, 1893–1910.
- Freitas, A. C. and Brahmananda Rao, V., 2011: Multidecadal and interannual changes of stationary Rossby waves. *Quart. J. Roy. Meteor. Soc.*, 137, 2157-2173.
- Gushchina, D., and Dewitte, B., 2019: Decadal modulation of the relationship between intraseasonal tropical variability and ENSO. *Climate Dynamics*, 52, 2091-2103.
- Henderson, S. A., E. D. Maloney, and S.-W. Son, 2017: Madden-Julian Oscillation Pacific Teleconnections: The Impact of the Basic State and MJO Representation in General Circulation Models. *J. Climate*, 30, 10.1175/jcli-d-16-0789.1, 4567-4587.
- Higgins, R. W., and W. Shi, 2001: Intercomparison of the principal modes of interannual and intraseasonal variability of the North American monsoon system. *J. Climate*, 14, 403–417.
- Hoskins, B. J., and Ambrizzi, T., 1993: Rossby wave propagation on a realistic longitudinally varying flow. *J. Atmos. Sci.*, 50, 1661-1671.
- Hoskins, B., Fonseca, R., Blackburn, M., & Jung, T., 2012: Relaxing the tropics to an ‘observed’ state: Analysis using a simple baroclinic model. *Quarterly Journal of the Royal Meteorological Society*, 138(667), 1618-1626.
- Jeong, J.-H., B.-M. Kim, C.-H. Ho, and Y.-H. Noh, 2008: Systematic Variation in Wintertime Precipitation in East Asia by MJO-Induced Extratropical Vertical Motion. *J. Climate*, 21, 788-801.
- Johnson, N. C., D. C. Collins, S. B. Feldstein, M. L. L’Heureux, and E. E. Riddle, 2014: Skillful Wintertime North American Temperature Forecasts out to 4 weeks Based on the State of ENSO and

- the MJO. *Wea. Forecasting*, 29, 23–38.
- Jones, C. and L. M. Carvalho, 2002: Active and Break Phases in the South American Monsoon System. *J. Climate*, 15, 905–914.
- Kang, W., and Tziperman, E., 2018a: The Role of Zonal Asymmetry in the Enhancement and Suppression of Sudden Stratospheric Warming Variability by the Madden–Julian Oscillation. *J. Climate*, 31, 2399–2415.
- , and ———, 2018b: The MJO-SSW Teleconnection: Interaction Between MJO-Forced Waves and the Midlatitude Jet. *Geophysical Research Letters*, 45, 4400–4409.
- Kessler, W., and R. Kleeman, 2000: Rectification of the Madden-Julian oscillation into the ENSO cycle. *J. Climate*, 13, 3560–3575.
- Kiladis, G. N., Dias, J., Straub, K. H., Wheeler, M. C., Tulich, S. N., Kikuchi, K., and Ventrice, M. J., 2014: A comparison of OLR and circulation-based indices for tracking the MJO. *Monthly Weather Review*, 142, 1697–1715.
- Kim, D., M.-I. Lee, H.-M. Kim, S. D. Schubert, and J. H. Yoo, 2014: The modulation of tropical storm activity in the Western North Pacific by the Madden–Julian Oscillation in GEOS-5 AGCM experiments. *Atmos. Sci. Lett.*, 15, 335–341.
- Klotzbach, P. J., 2010: On the Madden–Julian Oscillation–Atlantic Hurricane Relationship. *J. Climate*, 23, 282–293, <https://doi.org/10.1175/2009JCLI2978.1>
- Lin, J.-L., and Coauthors, 2006: Tropical intraseasonal variability in 14 IPCC AR4 climate models. Part I: Convective signals. *J. Climate*, 19, 2665–2690.
- Liu, Y., and Hsu, P. C., 2019: Long-term changes in wintertime persistent heavy rainfall over southern China contributed by the Madden–Julian Oscillation. *Atmospheric and Oceanic Science Letters*, 12, 361–368.
- Madden, R. A., and Julian, P. R., 1971: Detection of a 40–50 day oscillation in the zonal wind in the tropical Pacific. *J. Atmos. Sci.*, 28, 702–708.
- , and ———, 1972: Description of global-scale circulation cells in the tropics with a 40–50 day period. *J. Atmos. Sci.*, 29, 1109–1123.
- Maloney, E. D., and D. L. Hartmann, 2000: Modulation of eastern north Pacific hurricanes by Madden-Julian oscillation. *J. Climate*, 13, 1451–1460.
- , 2001: The Madden–Julian oscillation, barotropic dynamics, and North Pacific tropical cyclone

- formation. Part I: Observations. *J. Atmos. Sci.*, 58, 2545–2558.
- Matthews, A. J., B. J. Hoskins, and M. Masutani, 2004: The global response to tropical heating in the Madden-Julian oscillation during the northern winter. *Quart. J. Roy. Meteor. Soc.*, 130, 1991–2011.
- McPhaden, M. J., 1999: Genesis and evolution of the 1997–1998 El Niño. *Science*, 283, 950–954.
- , 2004: Evolution of the 2002/03 El Niño*. *Bull. Amer. Meteor. Soc.*, 85, 677–695, <https://doi.org/10.1175/BAMS-85-5-677>
- McPhaden, M. J., Lee, T., and McClurg, D., 2011: El Niño and its relationship to changing background conditions in the tropical Pacific Ocean. *Geophysical Research Letters*, 38.
- Mo, K. C., and R. W. Higgins, 1998: Tropical influences on California precipitation. *J. Climate*, 11, 412–430.
- , 2000: Intraseasonal modulation of summer precipitation over North America. *Mon. Wea. Rev.*, 128, 1490–1505.
- Moon, J.-Y., B. Wang, and K.-J. Ha, 2011: ENSO regulation of MJO teleconnection. *Climate Dyn.*, 37, 1133–1149.
- , 2013: Teleconnections associated with Northern Hemisphere summer monsoon intraseasonal oscillation. *Climate. Dyn.*, 40, 2761–2774.
- Naoe, H., Matsuda, Y., and Nakamura, H., 1997: Rossby wave propagation in idealized and realistic zonally varying flows. *Journal of the Meteorological Society of Japan*. 75, 687–700.
- , and Matsuda, Y., 1998: Rossby wave propagation and Nonlinear Effects in Zonally-Varying Basic Flows. *Journal of the Meteorological Society of Japan*. 76, 385–402.
- Pegion, K., and B. P. Kirtman, 2008: The Impact of Air-Sea Interactions on the Predictability of the Tropical Intraseasonal Oscillation, *J. Climate*, 21, 5870–5886.
- Pohl, B., and Matthews, A. J., 2007: Observed changes in the lifetime and amplitude of the Madden-Julian oscillation associated with interannual ENSO sea surface temperature anomalies. *J. Climate*, 20, 2659–2674.
- Roundy, P. E., 2014: Some Aspects of Western Hemisphere Circulation and the Madden-Julian Oscillation, *J. Atmos. Sci.*, 71, 2027–2039.
- Roxy, M. K., Dasgupta, P., McPhaden, M.J. et al., 2019: Twofold expansion of the Indo-Pacific warm pool warps the MJO life cycle. *Nature*, 575, 647–651.

- Sardeshmukh, P. D., 1988: The Generation of Global Rotational Flow by Steady Idealized Tropical Divergence. *J. Atmos. Sci.*, 45, 1228-1251.
- Seo, K.-H., and Y. Xue, 2005: MJO-related oceanic Kelvin waves and the ENSO cycle: A study with the NCEP Global Ocean Data Assimilation. *Geophys. Res. Lett.*, 32, L07712, doi: 10.1029/2005GL022511.
- , and Son, S. W., 2012: The global atmospheric circulation response to tropical diabatic heating associated with the Madden–Julian oscillation during northern winter. *J. Atmos. Sci.*, 69, 79-96.
- , and H.-J., Lee, 2017: Mechanisms for a PNA-Like Teleconnection Pattern in Response to the MJO. *J. Atmos. Sci.*, 74, 1767-1781.
- Simmons, A. J., 1982: The forcing of stationary wave motion by tropical diabatic heating. *Quart. J. Roy. Meteor. Soc.*, 108, 503-534.
- Simmons, A. J., J. M. Wallace, and G. W. Branstator, 1983: Barotropic wave propagation and instability, and atmospheric teleconnection patterns. *J. Atmos. Sci.*, 40, 1363–1392.
- Takayabu, Y. N., T. Iguchi, M. Kachi, A. Shibata, and H. Kanzawa, 1999: Abrupt termination of the 1997–98 El Niño in response to a Madden–Julian oscillation. *Nature*, 402, 279-282.
- Yoo, C., Feldstein, S., and Lee, S., 2011: The impact of the Madden-Julian Oscillation trend on the Arctic amplification of surface air temperature during the 1979–2008 boreal winter. *Geophysical Research Letters*, 38, L24804.
- Wheeler M. C., and H. H. Hendon, 2004: An all-season real-time multivariate MJO index: Development of an index for monitoring and prediction. *Mon. Wea. Rev.*, 132, 1917–1932.
- , and J. L. McBride, 2005: Australian–Indonesian monsoon. *Intraseasonal Variability in the Atmosphere–Ocean Climate System*, W. K. M. Lau and D. E. Waliser, Eds., Springer Praxis, 125–173.
- , H. H. Hendon, S. Cleland, H. Meinke, and A. Donald, 2009: Impacts of the Madden–Julian Oscillation on Australian Rainfall and Circulation. *J. Climate*, 22, 1482–1498.
- Xiaolong, J., C. Lijuan, R. Fumin, and L. Chongyin, 2011: Impacts of the MJO on Winter Rainfall and Circulation in China. *Adv. Atmos. Sci.*, 28, 521-533.
- Yasunari, T., 1979: Cloudiness fluctuations associated with the Northern Hemisphere summer monsoon. *J. Meteor. Soc. Japan*, 57, 227–242.
- Zhang, C., and J. Gottschalck, 2002: SST anomalies of ENSO and the Madden-Julian Oscillation in the

equatorial Pacific. *J. Climate*, 15, 2429-2445.

Zhou, S., M. L'Heureux, S. Weaver, and A. Kumar, 2012: A composite study of the MJO influence on the surface air temperature and precipitation over the Continental United States. *Climate Dyn.*, 8, 1459-1471.

Acknowledgement

유니스트 대학원에 입학하고, 또 마무리를 짓는 순간까지 많은 분들의 도움과 응원이 없었다면 저는 박사학위를 마무리할 수 없었을 것입니다. 이 자리를 빌어 그 분들에게 감사의 말을 전하고자 합니다.

먼저, 저의 지도 교수님이신 이명인 교수님께 제일 먼저 감사의 말씀을 드립니다. 너무나도 부족하고 철부지인 제가 박사 학위를 마무리를 질 수 있었던 것은 모두 교수님 덕분입니다. 지난 8 년간 교수님께 받은 끊임없는 지지와 가르침을 가슴 깊이 새기도록 하겠습니다. 그 가르침을 바탕으로 더 발전하는 과학자가 되도록 하겠습니다. 진심으로 감사합니다.

그리고 저의 박사학위 위원회 교수님이신 송창근 교수님, 차동현 교수님, 손석우 교수님, 김대현 교수님께도 이 자리를 빌어서 감사의 말을 드립니다. 발표 때마다 교수님들께서 해 주신 조언들은 제가 연구를 진행하고, 또 정리하는 데에 있어서 정말 큰 도움이 되었습니다. 교수님들을 제 박사학위 위원회로 모실 수 있어서 정말 영광이었습니다.

제가 대학원 생활을 하는 동안에 우리 기후환경모델링 연구실의 모든 분들의 도움을 받았습니다. 저의 대학원 선배님이시자 지금은 미국에서 포닥을 하는 동민오빠! 제 대학원 생활의 처음부터 끝까지 오빠의 도움이 없었던 적이 없네요. 정말 감사합니다. 그리고 연구실에서 언제나 저희들을 챙겨주시던 성윤오빠, 오빠가 어디에 계신든 언제나 응원하겠습니다. 2019 년에 처음 같이 연구실 생활을 하게 되었지만 그 누구보다 연구실 학생들을 챙겨주시는 이준리 박사님. 질문이 정말 많았었는데 언제나 친절하게 알려주셔서 정말 감사합니다. 지금은 시애틀에 있는 연구실의 분위기 메이커이자 선후배들을 살뜰히 챙기던 대현이, 다양한 연구 분야를 섭렵하여 연구 에이스인 은교, 연구실에서 환경 모델링의 에이스인 강한이, 연구실 만능엔터테이너이자 이제 연구실에서 제일 만리로 연구실 후배들을 돌보느냐 고생하는 낙빈이, 긴 시간 동안 연구실에서 같이 동고동락하며 지내서 이제 친동생같은 승희, 연구실의 재간동이 막내인 농구천재 선래, 만난 시간은 짧지만 많은 것을 같이 한 기숙사메이트 지해, 연구실의 막내였지만 지금은 능률하게 군복무를 하고 있는 민상이, 재치가 넘치던 귀염동이 선주, 다른 분야를 전공했지만 우리 연구실에 와서 누구보다 열심히 한 혁재, 함께 연구를 하면서 많은 것을 가르쳐 주셨던 박명숙 박사님, 그리고 연구실의 힘든 행정일을 모두

하시면서도 저희도 챙겨주시는 임지현 선생님. 모두에게 정말도 감사하고 고맙다는 말을 전하고 싶습니다.

연구 과제와 연구를 할 때, 물심양면으로 많은 도움을 주시고 또 응원해주신 국립기상과학원의 박사님들과 소민언니, 그리고 바쁜 시간을 내어 주셔서 태풍을 가르쳐 주신 시애틀의 문유민 박사님께 감사의 말씀을 전하고 싶습니다. 그리고 궁금한 것, 모르는 것이 있으면 언제나 친절하게 알려주시던 부산대학교 손준혁 선배와 이현주 언니, 그리고 많은 이야기를 하며 고민을 나누고 응원을 해준 박해리 언니. 정말 고맙습니다.

통계 계산이 막힐 때마다 연락해서 귀찮게 해도 언제나 쉽게 통계를 가르쳐 주시던 진영선배와 비록 다른 과이지만 먼저 대학원 생활을 마친 지언언니, 중학교 때 만나 지금까지 항상 내 곁에서 같이 슬퍼해주고 기뻐해주던 설아, 부산대학교 십이지 가족이자 내 동기들인 자령이, 은석이, 정길이, 멋진 약사님이신 태훈오빠와 내 정신적 지주인 현아언니. 시카고에서 제 박사과정 마무리를 응원해준 혜선이, 현준씨, 강성재 박사님. 모두가 있어서 끝날 것 같지 않았던 울산에서의 대학원 생활을 버틸 수 있었습니다. 정말 고맙습니다.

20 살 때부터 부산과 울산에서 지낸 딸을 언제나 걱정해주고, 챙겨주고 지지해주던 엄마, 아빠, 그리고 이제 두 애기의 엄마가 된 내 동생 명선이, 공부한다고 잘 챙겨드리지 못했지만 언제나 예뻐해주신 어머님과 아버님, 그리고 가끔 만나도 언제나 잘 챙겨주는 수아언니와 재혁이에게 감사하다는 말을 전합니다. 마지막으로, 20 살때부터 지금까지 내 옆에 있으면서 끊임없는 사랑과 믿음, 지지를 보내주는 내 남편, 봉서오빠에게도 고맙다고 말하고 싶습니다. 오빠와 함께한 대학원 생활은 평생 잊지 못할 꺼야.

여기에 다 언급하지는 못하였지만, 대학원 생활을 하면서 만나고, 함께 했던 모든 분들께 감사하다는 말을 하고 싶습니다. 이곳에서 배우고 쌓은 지식과 경험을 바탕으로 학계에 기여를 할 수 있는 과학자가 되도록 노력하겠습니다. 감사합니다.